SURFACE MORPHOLOGY IMPLICATIONS ON LANGMUIR PROBE MEASUREMENTS

by

Padmashri Suresh

A thesis submitted in partial fulfillment
of the requirements for the degree

of

MASTER OF SCIENCE

in

Electrical Engineering

Approved:

Dr. Charles M. Swenson Major Professor	Dr. Edmund A. Spencer Committee Member
Dr. Jan J. Sojka Committee Member	Dr. Byron R. Burnham Dean of Graduate Studies

UTAH STATE UNIVERSITY
Logan, Utah

2011

Abstract

Surface Morphology Implications on Langmuir Probe Measurements

by

Padmashri Suresh, Master of Science

Utah State University, 2011

Major Professor: Dr. Charles M. Swenson
Department: Electrical and Computer Engineering

Langmuir probes are extensively employed to study the plasmas in space and laboratory environments. Successful measurements require a comprehensive modeling of both the plasma environment and the probe conditions in the form of current collection models. In this thesis, the surface morphology implications on the probe current collection are investigated. This problem is applied and solved in the context of a CubeSat regime. The first problem that is investigated is the consequence of surface structural variability on the current measurements. A new model for dealing with non-uniformity of the probe surface structure is developed in this paper. This model is applied to analyze the Langmuir probe data from a sounding rocket mission that was subjected to surface structural non-homogeneities. This model would be particularly useful for CubeSat platforms where elaborate probe design procedures are not feasible. The second problem that is investigated is the surface area implications on Langmuir probe measurements. It has been established that surface area ratio of the spacecraft to that of the probe needs to be sufficiently large to make successful plasma measurements. CubeSats would therefore pose a challenge for employing Langmuir-type instruments to study the space plasma. We inspect the feasibility of making plasma measurements using Langmuir probes subjected to CubeSat area

constraints. This analysis is done for a forthcoming Utah State University (USU)/Space Dynamics Lab (SDL) CubeSat mission.

(100 pages)

To Mum, Dad, and dearest Sunny.....

Acknowledgments

It is my great pleasure to thank all the people who helped in accomplishing this work. First and foremost, I am grateful to my advisor, Dr. Charles Swenson, for his encouragement, support, and guidance. I will be forever indebted to him for suffering all my ignorant questions and letting me learn at my own pace. His enthusiasm and his passion towards space science have been a big influence on me. I consider myself to be extremely fortunate for having the privilege of working under his supervision.

I would also like to thank Dr. Edmund Spencer and Dr. Jan Sojka for their encouragement and insightful comments. I am also thankful to ECE graduate advisor, Mary Lee Anderson, for proofreading this thesis.

I would like to thank all my labmates for making EL 204 a great place to work. I would like to thank my friends Leeju, Kiran, Darshan, Sravanthi, and Sumana for their support through the ups and downs of my "thesis years."

I am thankful to my wonderful parents, Suresh and Prema, for their love and unwavering support, and for their faith in my abilities.

Last, but not the least, I thank the almighty for reasons too numerous to mention.

Padmashri Suresh

Contents

List of Tables

List of Figures

Chapter 1

Introduction

Langmuir probes have been an integral part of the plasma diagnostic process since the early 1920s. Pioneered by Irving Langmuir; these instruments have been used to study wide variety of plasma environments [1]. They have been successfully flown on numerous spacecraft missions to make in-situ measurements of the space plasmas, particularly the planetary ionospheres [2]. A high-level description of a Langmuir probe is an instrument consisting of a DC electrode immersed in the plasma being observed. The current collected by this electrode due to the interaction of the charge carriers present in the plasma, forms the basis for the measurement technique employed to gauge the plasma behavior.

Langmuir probes generally can be implemented in three different ways, determined by the properties of plasma that the experiment is set up to study. If the experiment is to characterize the relative density of a single species of charge carriers, fixed-bias DC probe implementation is used. In this realization, a constant voltage is applied to the electrode. The relative density of the charge carrier species in the plasma is determined from the current collected by the probe resulting from the constant bias voltage. If a fixed positive bias voltage is applied with respect to the spacecraft body and the spacecraft does not exhibit significant self-charging, the probe functions as an electron probe while a negative bias voltage results in an ion probe. If we wish to make measurements, characterizing both the electron and ion populations in the plasma, then the voltage applied to the probe is swept across a continuous range of values spanning both positive and negative bias. This type of implementation is known as the sweeping Langmuir probe which is often referred to as the SLP in Utah State University (USU) rocket experiments. In this mode, it is also possible to study the temperature or energy distribution of plasma and the surface charge of the experiment relative to the ambient plasma. The bias voltage is applied to the electrode

through a transimpedance amplifier, which along with a difference amplifier serves as the front end to an A/D converter.

The third type of implementation is the floating potential probe type, where the probe is not biased but is allowed to settle at the floating potential of the instrument. This configuration is particularly useful in studying spacecraft charging process. When used in the double probe configuration, electric field measurements can be made.

The current collected by a fixed bias probe is used to deduce only the relative density measurements. When operating in the sweeping mode, the temperature of the charge carrier of interest is deduced, in addition to the density. The process of determining these plasma characteristics from the current collected by the probe is a complex process determined by the inter-woven relationship between the probe design, the plasma behavior and the flight environment.

The process of current collection for a probe in plasma was first modeled by Langmuir [3] for the case of a stationary, collisionless plasma known as the orbital motion limited (OML) theory. This theory referred to as the OML theory, has been extended over the years for different plasma regimes and probe design constraints. Some of the enhancements to OML theory include: the modeling of current collection under collisional, non-drifting, unmagnetized plasma by Sanmartin [4], the modeling of current collection under drifting plasma conditions by Hoegy and Wharton [5], and Medicus [6]. Laframboise and Rubinstein [7] have tackled the case of adding magnetic field effects to the OML theory.

These theories of current collection also need to consider the flight environment which contributes to additional sources of current for the probe. A daytime flight would necessitate the addition of photoelectron interaction. This is particularly important in the low density space plasma environments where photoelectric current exceed the ion currents collected from the plasma.

Other flight considerations are dusty plasmas and radiation environments which also induce current collection dependencies. Factors like secondary emission backscatter and triboelectric charging [8] must be considered in these environments.

The surface morphology of the probe, i.e. the probe surface structure and the probe surface size, need to be included when defining the current collection process. Irregularity in surface structure and insufficient surface area available for collection are known to alter the normal process of current collection. We investigate the implications of the surface morphology on the current models for Langmuir probes in this thesis.

1.1 Surface Structure Implications

Structural properties of the probe surface influences the effective probe-plasma potential, and hence the current collected by the probe. The surface structure property of the probe is largely defined by the work function of the probe. Work function is the minimum amount of energy required to extract an electron from the surface and is given by the potential difference from the Fermi level to the vacuum [9–11].

Work function is influenced by two factors: the chemical potential and the surface potential. It can be expressed as: $\Phi = \triangle\Phi - \bar{\mu}$. In fig. 1.1, μ is the band-energy level of the atom, $\triangle\Phi$ is the energy level associated with electrostatic potential which varies along the surface fields and crystalline structure at the surface, and $\bar{\mu}$ is the chemical potential component.

Chemical potential is determined by the bulk properties of the material. The surface potential is determined by the dipole field structure on the surface. A change in the surface morphology brought about by adsorption of external agents, contaminants would change

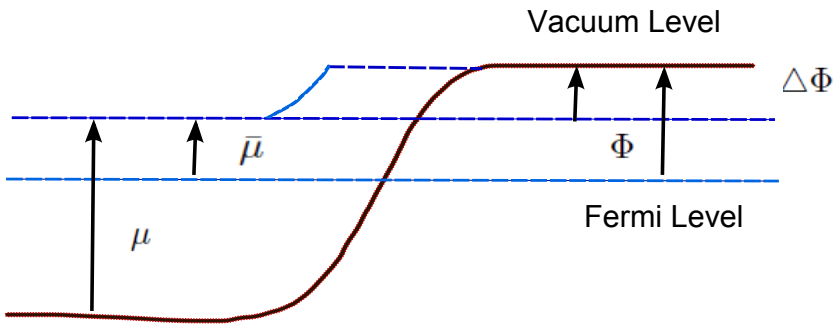

Fig. 1.1: Workfunction representation in terms of contributing potential levels (energy levels).

the surface field structure, thereby changing the work function. Work function changes are also brought about by physical and chemical process such as heating, oxidation, diffusion which alters the bulk properties. This variability in the surface behavior or work function of a Langmuir probe is ultimately manifested as a variation of the probe to plasma potential.

The standard experimental approach to ensure surface uniformity is to employ a two-fold design procedure consisting of suitable material selection and implementation of surface protection against contamination. Elements with smooth work function and chemical inertness like Gold and Graphite [12] have historically been used. In addition, TiN, as described by the results of Wahlstrom et al. [13] and M. Veszelei and E. Veszelei [14] is favored because of low surface granularity and high chemical stability, and has been used on a number of space probes.

Factors disturbing surface uniformity during the assembling and handling of the probe and those during flight are addressed with suitable in-flight protective measures like enclosing the probe in a vacuum chamber till deployment [15] or indirect heating of the probe in the atmosphere [16]. The experiment conducted by Amatucci et al. [17] has shown that Titanium nitride (TiN) and other surfaces heated in vacuum would boil-off any possible contaminants. Probes used in the study of laboratory plasma are subjected to energetic ion-bombardment to remove contaminants during the experiment.

However, it has been observed that design measures alone do not guarantee uniform surface conditions during flight. Thomas and Battle [18] observed this in the case of laboratory plasmas. Recontamination of cleaned probes was observed within a fraction of a second under atmospheric conditions. Also, implementing in-flight cleaning techniques is not always feasible or considered, making such probes highly susceptible to contamination during the launch and flight. Non-uniformity in the surface due to contamination effects have been reported by Hirt et al. [19] on the Langmuir probe onboard the DEOS F06 flight and by Steigies et al. [20] on the Langmuir probe onboard the CUSP and JOULE missions.

This problem of variations in the surface behavior despite the use of counter measures indicates that the current collection theory needs to account for these effects. The variability

in the surface behavior of a Langmuir probe is ultimately manifested as a variation of the probe to plasma potential.

A model given by Oyama [21] explains the process of current collection in the event of probe-plasma potential variation using a resistor-capacitor model. A correction algorithm to recover the true current-voltage (I-V) characteristic using this model has been given by Piel et al. [22]. This algorithm models the variation of plasma to probe potential across the surface as a homogeneous effect. The contaminant expected in this case was water vapor which mainly contributes to temporal variations as if desorbed from the surface of the probe. Hence, the spatial variations were considered to have been averaged-out over the surface. Such contaminants result in the upsweep and downsweep of the driving voltage to collect differently resulting in the hysteresis curve effect.

However, there could be cases where the contaminant is reactive with respect to the probe surface inducing spatial inconsistencies. This could also be the case when the probe material develops surface granularity induced by the factor causing the variation of surface behavior or when the probe material is inherently granular. In such cases, we would have to embed the spatial non-uniformity into current collection model. The spatial surface behavior could be completely characterized by the work function of the surface under consideration. In this thesis, we use work function variation to model the spatial non-uniformities of the probe surface.

1.2 Surface Area Implications

The surface area of the probe when small in comparison to that of the spacecraft body, is known to cause fluctuations in the spacecraft ground, resulting in skewed I-V curves. It has been noted that spacecraft bodies which are not bigger than the probe body by a factor of 1000 [23] are known to suffer from alterations in the plasma property calculations. CubeSats, with their small surface area, impose limitations on available return current for Langmuir probes. When the probe is collecting electron currents, the spacecraft needs to have a sufficiently large surface area for collecting ions due to the relatively lesser magnitude of the ion current. If the area is not sufficient, to balance out the probe current collection,

the spacecraft reference potential swings more negative. This nonlinear collection and return currents are bound to charge the CubeSat and complicate the measurement of the plasma properties. The effects of such an effect would be particularly severe when the probe is operating at a fixed mode collecting electrons. It has been noted in sounding rocket mission measurements with a spacecraft to probe ratio of 250 [24] that the probe does not operate successfully in the fixed mode and when being swept, temperature gets overestimated.

CubeSats with their small form factor are bound to be effected by this problem. We use a PSPICE software based tool to simulate the current collection process for CubeSats and investigate the dynamics of Langmuir probe spacecraft interactions. In this thesis, we present simulations and findings on the possibility of making accurate measurements from Langmuir probes subjected to the CubeSat regime design constraints.

1.3 Storms Mission Overview

On October 30, 2007 NASA launched rocket 36.218 carrying the mission: "Investigation of Mid Latitude Ionospheric Irregularities Associated with Terrestrial Weather Systems" also known as the STORMS Mission seen in fig. 1.2. The rocket was launched from Wallops Island, Virginia (37.95° N, 284.53° E, 67.5° dip angle) at twelve minutes past local midnight. It flew along an azimuth of 114° and reached apogee near 394 km.

The STORMS mission was launched to investigate the phenomenon of spread-F at mid latitudes. The Earth's ionosphere is highly dynamic: subjected to wide variety of structural and temporal irregularities and perturbations [25,26]. The non-uniformity in the F region which causes the transmitted radio waves to register as diffused echoes on the high frequency receiver has been studied as the phenomenon of spread-F. The non-uniform F region causes the radio waves to bounce back with varied phase and signal strength and from different heights and location causing the echoes to appear as diffused thick traces on the high frequency sounders [27]. They exhibit a many-to-many-set mapping of the virtual height and the transmitted frequency leading to the classification of this ionospheric phenomenon into two types: range spread and frequency spread based on the reflected trace signature, as seen in the fig. 1.3 [28].

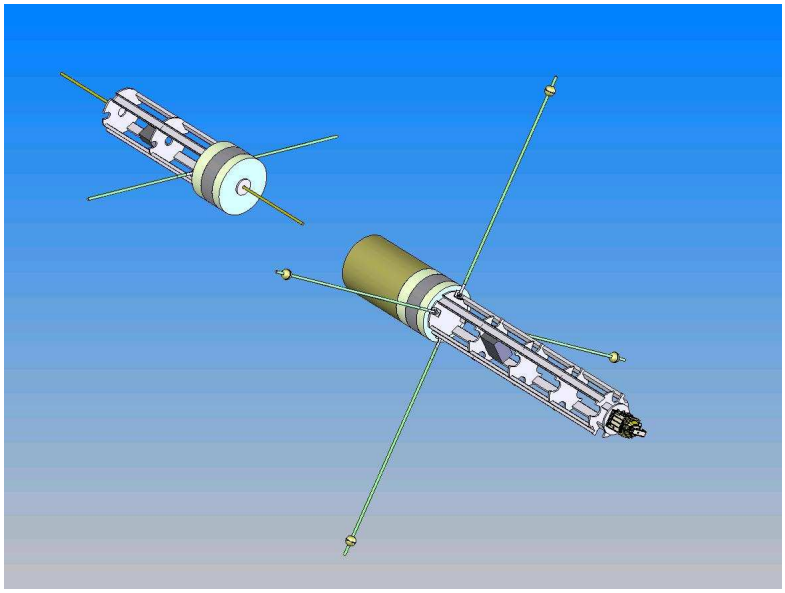

Fig. 1.2: STORMS payload.

The state of the ionosphere when either of these two spread types is seen has mostly been linked to plasma instabilities and the presence of wave motion in the ionosphere. Both acoustic gravity waves and magnetospheric waves are studied as possible causes. Instabilities like Rayleigh-Taylor's instability, Perkin's instability, and Es-F region coupling aided instability are prominently associated with the spread-F event. The spread-F phenomenon is known to occur extensively at high and low latitudes but at a relatively lesser incidence at mid latitudes. To gain further insight into the spread-F at geomagnetic mid latitudes termed as mid latitude spread-F was the scientific objective of this mission. This mission happens to be unique due to the fact that, this sounding rocket data presents the first in-situ observation of the spread-F phenomenon at mid latitudes.

The scientific payload consisted of a mother-daughter configuration with instrument provided by the University of Texas-Dallas and Utah State University/Space Dynamics Lab. The main payload instruments built by University of Texas-Dallas included a Hanson Anemometer for Thermospheric Investigations (HATI) to measure neutral winds and a Vector Electric Field Instrument (VEFI) to measure quasi-DC electric fields, the discussion and data analysis of which can be found elsewhere [29]. The daughter payload designed

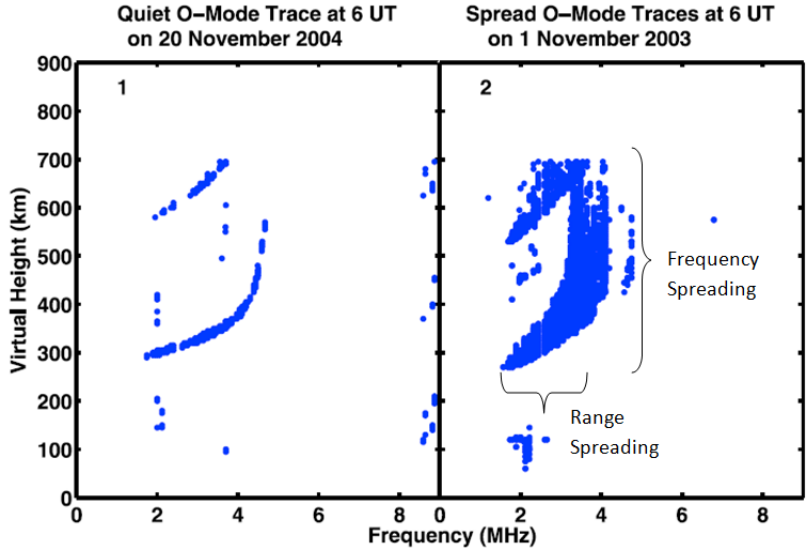

Fig. 1.3: Spread-F seen on the ionosonde at Wallops Island.

by Utah State University included a suite of instruments to measure relative and absolute electron density, electron-neutral collision frequency, temperature, and electric field. It consists of Plasma Frequency Probe (PFP), swept impedance probe (SIP), and DC Langmuir Probe (DCP) sensors, collectively called as the plasma impedance probe (PIP). There is also a Sweeping Langmuir Probe (SLP) sensor and four Floating Potential Probe (FPP) sensors separated from one another by 90°. In this paper we concentrate mainly on the SLP and its measurements. The FPP and SIP data provide supplementary information to complete the SLP data analysis.

The sweeping Langmuir probe was a cylindrical probe swept from -1 to 3 volts every 20 seconds during the flight and maintained at 3V otherwise. Thus, SLP makes continuous density measurements and makes periodic temperature measurements when operating in the sweeping mode. The SLP was designed with a coating of TiN and was preheated to 200° for 90 minutes prior to launch, to ward-off any effects of contamination. However, the probe on heating exhibited an interesting surface behavior, as seen in the fig. 1.4.

The first probe in fig. 1.4 is the one which is heated to 200° and the one below is prior to heating. As observed from the image there is non-uniformity in the surface

Fig. 1.4: STORMS SLP probe: Before and after heating.

characteristics of the probe, post heating. The alteration of surface behavior on heating indicates a structural change due to a change in the bulk properties of the metal, causing a work function change. Though TiN is considered to be chemically inert and subjected to minimum inherent work function variation, the presence of visible non-homogeneity on the probe surface suggests a spatially varying current collection process caused by an external process such as contamination.

As observed in this mission, uniform surface behavior of the probe despite favorable design features indicates the necessity of using modeling techniques during the analysis of the probe.

1.4 Thesis Overview

This thesis is organized and presented in six chapters. Chapter 1 presented a review of the relevant Langmuir probe literature and an overview of the STORMS mission. Chapter 2 presents the development of the model and current collection equations. The data from the STORMS mission is presented in Chapter 3, where the extraction, formatting, and verifying the suitability of the rocket data is presented. The equations developed in Chapter 2 are applied to the SLP data from the STORMS mission to analyze the ionospheric plasma. The curve fitting results, density and temperature findings are presented in Chapter 4.

Chapter 5 deals with the study of suitability of Langmuir probe measurements for use on small area spacecrafts. We investigate the surface area implications for a probe onboard a CubeSat form-factor spacecraft. Chapter 6 presents the conclusion and the suggested future developments and research from the work presented in this thesis.

Chapter 2

Current Collection Model for Surface Structure Variations

The current collected by an unbiased Langmuir probe is solely due to the random motion of charge carriers intercepted by the surface area of the body and is given by

$$I_{\mathrm{th_j}} = AJ_{\mathrm{th_j}}, \tag{2.1}$$

where $J_{\mathrm{th_j}}$ = Thermal current density of charge carrier species j, given by

$$J_{\mathrm{th_j}} = ANq_j\sqrt{\frac{K_{\mathrm{b}}T}{2\pi M_j}}, \tag{2.2}$$

where A is the area of the collecting body, N is the density, q_j is the electric charge of the carrier species, K_{b} is the Boltzmann constant, T is the temperature, and M_j is the mass of the charge carrier species. This expression is commonly called as thermal current or random current.

When a bias voltage is applied to the probe, the current collection is more complicated and is dependent on the plasma regime, plasma sheath, and bias voltage conditions. The current collected by such a probe can be studied as three different regions based on the bias voltage in relation to the potential of the surrounding plasma.

This can be seen in fig. 2.1 which illustrates the current collected by a Langmuir probe immersed in a plasma and biased relative to the ambient plasma for unit area (current density). When the bias voltage is negative with respect to the plasma, the probe is primarily collecting positive ions and the part of I-V curve which corresponds to this collection is called the ion saturation region.

As the bias on the body becomes less negative, some electrons which have sufficiently

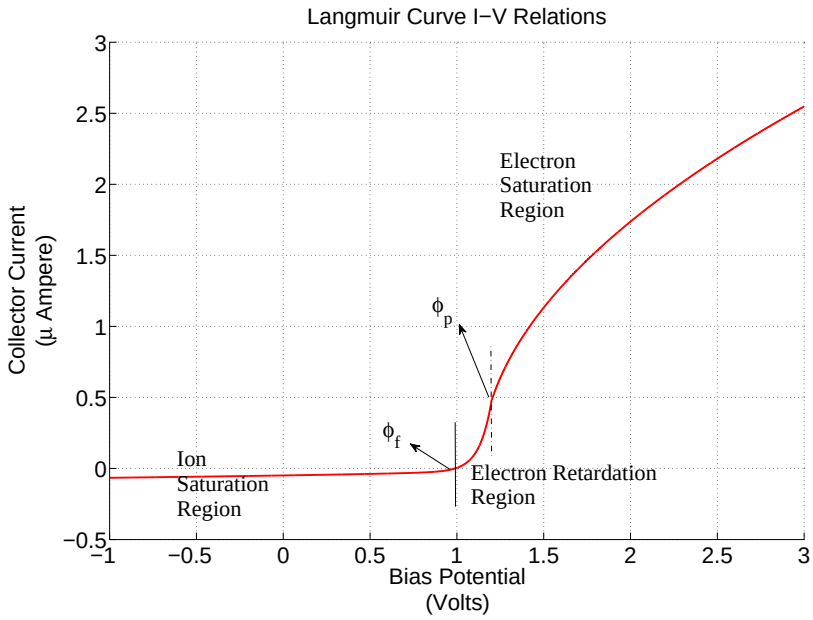

Fig. 2.1: Langmuir curve I-V relations.

large energy, overcome the energy barrier of the bias voltage and get collected by the probe. The region of the I-V curve corresponding to such behavior of positive ion collection with the inclusion of high energy electron collection is called the electron retardation region. The transition between the ion saturation region and electron retardation region occurs at the point called the floating potential which corresponds to the voltage where the current due to positive ions and electrons are balanced leading to zero current collection by the body immersed in the plasma. As the bias sweep becomes increasingly positive, it reaches a stage when it is larger than the potential of the surrounding plasma. This leads to the body primarily collecting electrons, and the point where the probe bias equals the potential of the surrounding plasma is called the plasma potential, and the I-V curve at greater potentials is known as the electron saturation region. In this region, only positive ions which have sufficiently high energy are collected, analogous to the electron collection in the electron retardation region. This ion current is effectively negligible due to the low order of the ion current magnitude in comparison with the electron current.

The equations describing the current collection process are presented in the next section. The current collected due to both positive and negative charge carriers is described by the same set of equations, except for a change of sign on the charge of the carrier species.

2.1 Current Equations for a Biased Langmuir Probe

The current collected by a biased probe due to a particular charge carrier species can be expressed as a piecewise function of the probe to plasma energy ($\Psi = q_j\Phi$). The current collection due to a particular charge carrier species can be defined as

$$I_j = f(\psi) = \begin{cases} I_{\mathrm{th_j}} \exp \frac{q_j\Phi}{\mathrm{C}} & \text{if } q_j\Phi < 0 \\ I_{\mathrm{th_j}} \left(\mathrm{P1} + q_j\Phi/\mathrm{P_2}\right)^{\beta} P3 & \text{otherwise.} \end{cases} \tag{2.3}$$

The exponential part of the piecewise current collection function, defined above, gives the retardation region current of the charge carrier of interest. This current is solely influenced by the probe to plasma potential and the thermal energy of the charge carriers. On substituting the thermal energy component into the exponential function

$$I_{\mathrm{ret_j}} = I_{\mathrm{th_j}} \exp\left(\frac{q_j\left(\phi - \phi_p\right)}{K_{\mathrm{b}}T}\right), \tag{2.4}$$

where $I_{\mathrm{ret_j}}$ is the retardation region current, ϕ is the bias voltage applied to the probe, ϕ_p is the plasma potential. The plasma potential ϕ_p and the probe potential ϕ are referenced in this expression to an arbitrary common point. This highlights the important physics that depends on the probe-to-plasma potential. It also acknowledges the engineering convention to place the reference point for plasma instrumentation electronics at the negative point of the power supply which is commonly tied to the skin of the spacecraft.

When the bias voltage is attractive towards a charge carrier, the current collection process is defined by the power law part of the current collection function defined in equation (2.3). The scaling exponent β gets determined by the effective area of current collection. The other two variables are determined by the plasma regime conditions. The effective area of current collection is determined by the probe size and geometry. The probe size

in relation to the size of the surrounding sheath determines whether the curvature of the probe gets factored out into the effective collection area. The sheath size to probe size ratio, when close to unity, is called as the thin sheath condition or as the sheath limited case. Here the probe collects charges as if it were an infinitely flat collector with the collection area being equal to the physical area projected for collection. Hence, the current collected is the thermal current defined by equation (2.1).

When the sheath size is larger than that of the probe, we have the thick sheath case or the orbital motion limited case. Here the effective collection area is a factor of the probe curvature. Instead of saturating to the thermal current, the current increases as a factor of the probe to plasma potential Φ. The rate of increase or the scaling exponent β in equation (2.3) is a function of the probe geometry. The planar collector collects like an infinitely flat collector collecting thermal current. However when the probe has a curvature, the probe is subjected to an increase in the effective area of collection due to the expanding sheath with rise of potential above the plasma potential.

The probe regime factors P_1, P_2, P_3 in the equation (2.3) are influenced by the plasma characteristics like magnetic field, drift velocity, gyroradius, pressure, etc. Owing to these variations of the exponent and the scaling multipliers of the current collection function in the saturation region, there are multiple representations of the current collection process, which are contingent upon the probe engineering and plasma features.

The most commonly encountered plasma behavior on Earth's ionospheric spaceflight based Langmuir probes is collisonless, Maxwellian, and with negligible geomagnetic field effects. However, the plasma gets classified as drifting or otherwise based on the charge carrier of interest. The electrons being less massive result in the ratio of probe speed (8Km/sec) to that of the electrons to be around 0.04 for a temperature of 1000K. On the other hand 1000K ions with mass ranging from 1 to 28 have the speed ratio to be between 2 to 10. The fast moving electrons can therefore be classified as being in a non-drifting Maxwellian plasma regime. The massive ions on the other hand, result in the plasma behavior to be that of a drifting-Maxwellian leading to the dominance of ion collection in

the ram direction of the probe. This condition, known as mesothermal plasma, results in the current collection function being solved separately for the ions and electrons due to a difference in their plasma regime definition. The non-drifting current collection is modeled using the OML theory [3] by Mott-Smith and Langmuir, whereas the collection theory with superimposed drift has been modeled by Hoegy and Wharton [5] for cylindrical probes and by Medicus [6] and Katz et al. [30] for a sphere. The scaling factors for the current collection function in the saturation region and the resulting current collection expressions are presented next in table 2.1, for different geometries.

The flat plate geometry refers to the thin sheath current collection of all geometries and thick sheath collection of planar conductors. The ion saturation region which is a drifting-Maxwellian collection is defined in the following table. Here the plasma regime factors need to account for the dominance of the drift velocity scaling on the current collection. The equations are defined in table 2.2.

In table 2.2, q_i is the ion charge, v_d refers to the drift velocity of the ions, and $v_{\mathrm{th_i}}$ refers to the ion thermal velocity.

The current collection described by the above defined equations in plotted in the I-V curves seen in fig. 2.2. This current is the total current I which is the sum of ion and electron currents. The current collection equations for the different plasma regimes could be similarly described by substituting the appropriate plasma regime factors P_1, P_2, and

Table 2.1: Electron collection.

Plasma regime: maxwellian, non-drifting, collisionless, non-magnetized		
Geometry	Scaling Factors	Current Collection
Flat Plate	$\beta = 0$ $\mathrm{P}_1 = 0, \mathrm{P}_2 = 0$ $P_3 = 1$	$I_{\mathrm{th_e}}$
Cylindrical	$\beta = 1/2$ $P_1 = 1, P_2 = K_b T$ $P_3 = \frac{2}{\sqrt{\pi}}$	$I_{\mathrm{th_e}} \frac{2}{\sqrt{\pi}} \left(1 + q_e \left(\phi - \phi_p\right) / K_b T\right)^{1/2}$
Spherical	$\beta = 1$ $P_1 = 1, P_2 = K_b T$ $P_3 = 1$	$I_{\mathrm{th_e}} \left(1 + q_e \left(\phi - \phi_p\right) / K_b T\right)$

Table 2.2: Ion ram currents.

Plasma regime: maxwellian, drifting, collisionless, non-magnetized		
Geometry	Scaling factors	Current collection
Flat Plate	$\beta = 0$ $P_1 = 0, P_2 = 0$ $P_3 = \frac{2\sqrt{\pi}v_d}{2v_{\mathrm{th_i}}}$	ANq_iv_d
Cylindrical	$\beta = 1/2$ $P_1 = 1 + \frac{2K_bT}{m_iv_d^2}$ $P_2 = \frac{1}{2m_iv_d^2}, P_3 = \frac{v_d}{v_{\mathrm{th_i}}}$	$\frac{ANq_iv_d}{\pi}\left(1 + \frac{2q_i(\phi-\phi_p)}{m_iv_d^2} + \frac{K_bT}{m_iv_d^2}\right)^{1/2}$
Spherical	$\beta = 1$ $P_1 = 1 + \frac{2K_bT}{m_iv_d^2}$ $P_2 = \frac{1}{2m_iv_d^2}, P_3 = \frac{2v_d}{v_{\mathrm{th_i}}}$	$ANq_iv_d\left(1 + \frac{2q_i(\phi-\phi_p)}{m_iv_d^2} + \frac{K_bT}{m_iv_d^2}\right)$

P_3.

In the next section, we investigate the behavior of the current collection function in the event of the variation of the function range - 'Φ' induced by the work function variance.

2.2 Current Collection Model for Probes with Non-Uniform Surface Structure - Work Function Variation Model

2.2.1 Model Development

The current collection equations presented so far are defined based on constant plasma to probe potential for a given value of bias voltage. This is not the case when the probe is prone to contamination and such factors that can be characterized as the variance of the work function of the probe surface. A spatially irregular probe or a spatially varying work function gets translated as a spatially fluctuating probe to plasma potential.

Spatially varying probe to plasma potential results in a spatially varying current collection. These currents can be modeled as an ensemble of collectors spread across the probe surface. Each of these collectors, which have a particular probe to plasma potential, have a distinctive work function. The measure of the work function dictates the kind of charge interaction occurring at the surface, and hence the amount of current collected. This results

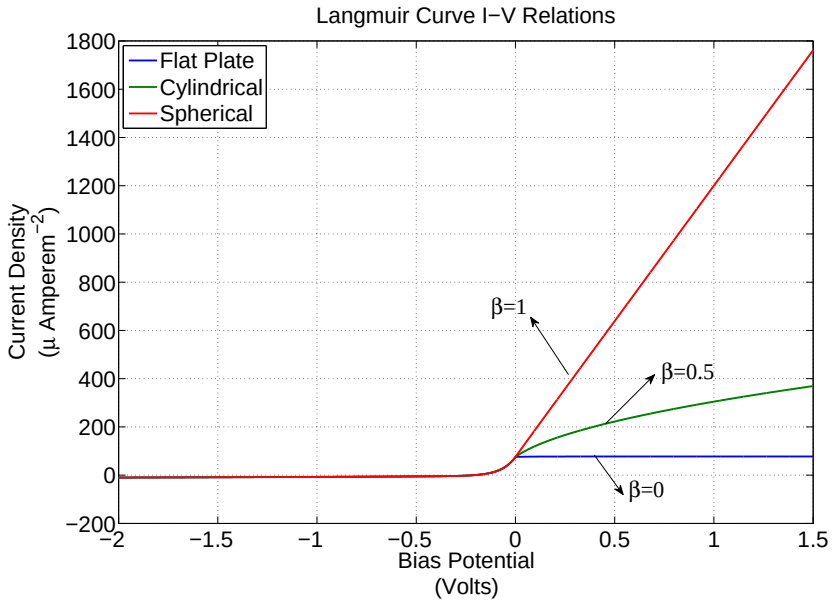

Fig. 2.2: Langmuir curve I-V relations.

in the probe behavior to be as if each of the small area of the probe surface corresponding to a particular work function were an independent probe.

This behavior of the probe surface could be best represented by denoting the spatially varying work function and the projected area of collection corresponding to each work function as two random variables. The term Φ is no longer a constant across the surface but is given by: $\Phi = \phi - \phi_p + \phi_w$, where the term ϕ_w is the random variable, denoting the work-function spread across the probe surface. The area mapping the work function spread can be represented by another random variable A_w.

The work function variance is a phenomenon that be scaled to the atomic level of the surface structure. This would imply that the area of collection mapping to the work function spread can be assumed to have negligible variance. In other words, each of the individual collecting surfaces with a particular work function could be considered to be collecting with same area.

The two random variables ϕ_w and A_w are uncorrelated since the influence of either of the variables on the other is absent and are hence statistically independent.

If ϕ_w and A_w can have n trials, or if there are n number of spatially varying collecting

surfaces spread across the probe, each of them will collect current as described by the current collection function of equation (2.3). Each of these collecting surfaces with a particular function will have all the attributes of the current collection function to be the same for a sweep of the probe bias voltage under consideration.

Figure 2.3 has the pictorial representation of a probe with spatially varying surface modeled as n separate collectors and the resulting current collection process in fig. 2.4, where each curve is described by the current collection process described by equations for a cylindrical probe in table 2.1 and table 2.2. Here we have assumed each of the individual collectors have the same area.

Since there are n collectors, we can represent the current collection function for a particular charge carrier species, with the work function variation embedded into the function definition as:

$$\sum_{k=1}^{n} g_1\left(\Phi = \phi - \phi_p + \phi_{w_k}\right) g_2\left(A_{w_k}\right), \tag{2.5}$$

where $g_1\left(\Phi = \phi - \phi_p + \phi_{w_k}\right) g_2\left(A_{w_k}\right)$ is the current collection function describing the process of current collection in the event of non-uniform work function(non-uniform probe to plasma potential). In the next section, we solve the current collection function for the work function variation model defined in equation (2.5) for the ionospheric plasma regime of the Earth.

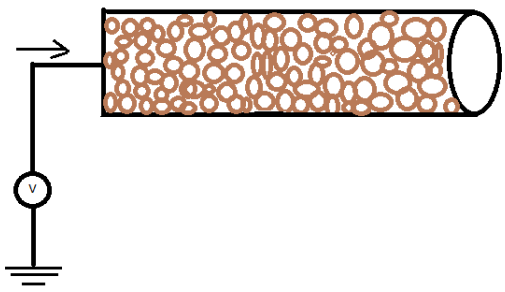

Fig. 2.3: Spatially varying current collection on a langmuir probe.

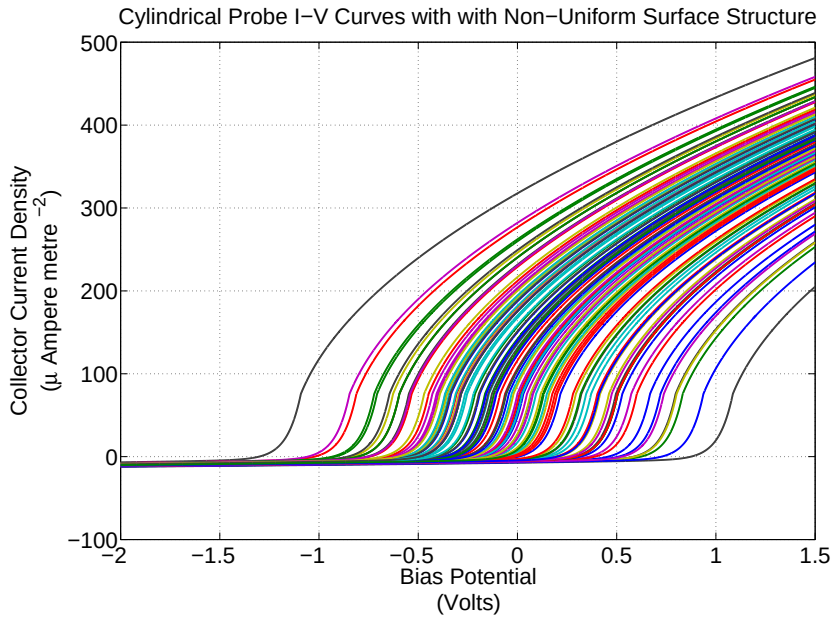

Fig. 2.4: Langmuir probe I-V curves for spatially varying current collection.

2.2.2 Current Collection Equations

The first step in solving the current collection function $g_1\left(\Phi = \phi - \phi_p + \phi_w\right) g_2\left(A_{w_k}\right)$ is to define the distribution type of the random variables. We choose ϕ_w to be a normally distributed random variable with mean $\mu = 0$ and standard deviation being σ. The distribution function is chosen to be Gaussian since the work function variation is expected to be mostly symmetrically centered on the mean. Since the function domain is at the atomic range, the area corresponding to each of the work function can be approximated to be equal or to be collecting in a similar manner. This means the A_w is a single valued random variable or could also be assumed to be normally distributed with $\sigma = 0$ and $\mu = 0$.

The surface structure non-uniformity being scaled at the atomic level results in large number of individual collecting areas. Hence, the number of trials n of the random variable is expected to tend to ∞. Therefore, we can write the current collection function as:

$$I_j = \lim_{n\to\infty} \sum_{k=1}^{n} g_1\left(\Phi = \phi - \phi_p + \phi_{w_k}\right) g_2\left(A_{w_k}\right), \tag{2.6}$$

where $g_1\left(\Phi = \phi - \phi_p + \phi_{w_k}\right)$ is the current collection function component of the probe to

plasma potential attribute and the $g_2\left(A_{w_k}\right)$ is the area attribute function. Since the individual collecting areas are equal to

$$\lim_{n\to\infty}\sum_{k=1}^{n} g_2\left(A_{w_k}\right) = A, \tag{2.7}$$

where A is the area of the probe projected for collection. Hence, equation (2.6) can be written as

$$I_j = A\lim_{n\to\infty}\sum_{k=1}^{n} g_1\left(\Phi = \phi - \phi_p + \phi_{w_k}\right). \tag{2.8}$$

When a random variable has large number of trials, the outcome of the random experiment is expected to tend to settle at the expectation or mean of the random variable. Hence, the equation (2.8) on applying the law of large numbers becomes

$$I_j = AE\left[g_1\left(\Phi = \phi - \phi_p + \phi_w\right)\right], \tag{2.9}$$

where $E\left[g_1\left(\Phi = \phi - \phi_p + \phi_w\right)\right]$ is the expectation or mean of the current collection function. From equation (2.3), we know that the current collection function actually expands out into a piecewise function of the probe to plasma potential Φ. The piecewise notation of equation (2.9) becomes

$$I_j = \begin{cases} I_{\mathrm{th_j}} E\left[\exp\left(\frac{q_j(\phi-\phi_p+\phi_w)}{C}\right)\right] & \text{if, } q_j\left(\phi-\phi_p+\phi_w\right) < 0 \\ \\ I_{\mathrm{th_j}} E\left[P1 + \left(\frac{q_j(\phi-\phi_p+\phi_w)}{P2}\right)^{\beta} P3\right] & \text{otherwise.} \end{cases} \tag{2.10}$$

Note that in the above equation, the Area A from equation (2.9) gets factored out into the thermal current component I_{th}. We first solve the piecewise function in the $q_j\left(\phi-\phi_p+\phi_w\right) < 0$ range to deduce the retardation region current, which is given by

$$I_{\mathrm{ret_j}} = I_{\mathrm{th_j}} E\left[\exp\left(\frac{q_j\left(\phi-\phi_p+\phi_w\right)}{C}\right)\right]. \tag{2.11}$$

On evaluating the expectation operator on the Gaussian random variable ϕ_w, we get

$$I_{\mathrm{ret_j}} = I_{\mathrm{th_j}} \frac{1}{\sigma\sqrt{2\pi}} \int_{-\infty}^{-\phi+\phi_p} \exp\left(\frac{q_j\left(\phi-\phi_p+\phi_w\right)}{C}\right) \exp\left(\frac{-\phi_w^2}{2\sigma^2}\right) d\phi_w. \tag{2.12}$$

We can reduce the integral to an analytical formula by re-arranging the indices of the exponential and reversing the integral limits,

$$I_{\mathrm{ret}} = I_{\mathrm{th}} \exp\left(\frac{q_j\left(\phi-\phi_p\right)}{C} + \frac{\sigma^2}{2C^2}\right) \left[1 - \frac{1}{\sigma\sqrt{2\pi}} \int_{-\infty}^{-\phi+\phi_p} \exp\left(\frac{\left(q_j\phi_w + \sigma^2/C^2\right)}{2\sigma^2}\right) d\phi_w\right]. \tag{2.13}$$

The integral evaluates into an Q-function variant

$$I_{\mathrm{ret}} = I_{\mathrm{th}} \exp\left(\frac{q_j\left(\phi-\phi_p\right)}{C}\right) \left[Q\left(\frac{q_j\left(\phi-\phi_p\right)+\sigma^2/\mathrm{C}}{\sigma}\right)\right], \tag{2.14}$$

where Q is the Q-function operator. On substituting the thermal characteristics K_bT into the above equation

$$I_{\mathrm{ret_j}} = I_{\mathrm{th_j}} \exp\left(\frac{q_j\left(\phi-\phi_p\right)}{K_bT}\right) \left[Q\left(\frac{q_j\left(\phi-\phi_p\right)+\sigma^2/\mathrm{K_bT}}{\sigma}\right)\right]. \tag{2.15}$$

The saturation region expressions have different representations for different plasma regime factors. We solve the generic case and substitute the appropriate scaling values under the different plasma conditions. The saturation region expression part of the current collection function is of the form

$$I_{\mathrm{sat_j}} = I_{\mathrm{th_j}} E\left[P1 + \left(\frac{q_j\left(\phi-\phi_p+\phi_w\right)}{P2}\right)^{\beta} P3\right]. \tag{2.16}$$

On evaluating the expectation operator on the Gaussian random variable ϕ_w, we get

$$I_{\mathrm{sat_j}} = I_{\mathrm{th_j}} \frac{1}{\sigma\sqrt{2\pi}} \int_{-\phi+\phi_p}^{\infty} \left(P1 + \left(\frac{q_j\left(\phi-\phi_p+\phi_w\right)}{P2}\right)^{\beta} P3\right) \exp\left(\frac{-\phi_w^2}{2\sigma^2}\right) d\phi_w. \tag{2.17}$$

The above expression is the generic form of the saturation region current. The integral evaluated to a closed form solution only when the scaling factor β is 0 or 1. We get Q-

Function representations similar to the retardation region. In all other cases, the numerical representation with the approriate scaling factors put in to P_1,P_2, and P_3 will represent the current collection equation.

The electron current collection for a plasma regime defined as Maxwellian, non-drifting, collisionless, non-magnetized, is solved for analyzing the current collection using the equation (2.17). Here the plasma regime factors are due to the applied potential and the sheath size behavior in response to the applied bias potential. The equations for electrons are defined in table 2.3 and table 2.4 for the ions.

Now the ion collection in the saturation region for a mesothermal condition is solved. The plasma regime factors are dependent on the ion drift velocity v_d.

The equations derived in this section described the current collected by a particular charge species only. The total current collected by the probe is the sum of the current collected by both the ion and electron charges.

2.3 Implications of Surface Structure Variations on Current Collection

We illustrate the I-V characteristics from the simulation of work function variation

Table 2.3: Electron collection: Work function variation theory.

Plasma Regime: Maxwellian, non-drifting, collisionless, non-magnetized		
Geometry	Scaling Factors	Current Collection ($I_{\mathrm{sat_e}}$)
Flat Plate	$\beta = 0$ $P_1 = 0$ $P_2 = 0$ $P_3 = 1$	$I_{\mathrm{th_e}} \left[1 - Q\left(\frac{q_e(\phi-\phi_p)}{\sigma}\right)\right]$
Cylindrical	$\beta = 1/2$ $P_1 = 1$ $P_2 = K_bT$ $P_3 = \frac{2}{\sqrt{\pi}}$	$I_{\mathrm{th_e}} \frac{1}{\sigma\sqrt{2\pi}} \int_{(-\phi+\phi_p)}^{\infty} \frac{2}{\sqrt{\pi}} \left(1 + \frac{q_e(\phi-\phi_p+\phi_w)}{K_bT}\right)^{0.5} \exp\left(\frac{-\phi_w^2}{2\sigma^2}\right) d\phi_w$
Spherical	$\beta = 1$ $P_1 = 1$ $P_2 = K_bT$ $P_3 = 1$	$I_{\mathrm{th_e}} \left[\left(1 + \frac{q_e(\phi-\phi_p)}{K_bT}\right) Q\left(\frac{q_e(\phi-\phi_p)}{\sigma}\right)\right] + I_{\mathrm{th_e}} \left[\frac{q_e\sigma}{2\sqrt{\pi}K_bT} \exp - \left(\frac{(\phi-\phi_p)^2}{\sqrt{2}\sigma}\right)^2\right]$

Table 2.4: Ion collection: Work function variation theory.

Plasma regime: Maxwellian, drifting, collisionless, non-magnetized		
Geometry	Scaling Factors	Current Collection
Flat Plate	$\beta = 0$ $P_1 = 0$ $P_2 = 0$ $P_3 = \frac{2\sqrt{\pi}v_d}{2v_{\mathrm{th_i}}}$	$ANq_iv_d\left[1 - Q\left(\frac{q_i(\phi-\phi_p)}{\sigma}\right)\right]$
Cylindrical	$\beta = 1/2$ $P_1 = 1 + \frac{2K_bT}{m_iv_d^2}$	$\frac{ANq_iv_d}{\pi}\frac{1}{\sigma\sqrt{2\pi}}\int_{(-\phi+\phi_p)}^{\infty}\frac{2}{\sqrt{\pi}}\left(1 + \frac{q_i(\phi-\phi_p+\phi_w)}{m_iv_d^2} + \frac{K_bT}{m_iv_d^2}\right)^{0.5}$
	$P_2 = \frac{1}{2m_iv_d^2}$ $P_3 = \frac{v_d}{v_{\mathrm{th_i}}}$	$\exp\left(\frac{-\phi_w^2}{2\sigma^2}\right)d\phi_w$
Spherical	$\beta = 1$ $P_1 = 1 + \frac{2K_bT}{m_iv_d^2}$ $P_2 = \frac{1}{2m_iv_d^2}$ $P_3 = \frac{2v_d}{v_{\mathrm{th_i}}}$	$ANq_iv_d\left[\left(1 + \frac{q_i(\phi-\phi_p+\phi_w)}{mv_d^2/2} + \frac{KbT}{mv_d^2/2}\right)Q\left(\frac{(\phi-\phi_p)}{\sigma}\right)\right.$ $\left. + \frac{q\sigma}{2\sqrt{\pi}mv_d^2/2}\exp - \left(\frac{-\phi_w^2}{\sqrt{2}\sigma}\right)^2\right.$

driven current collection of a cylindrical probe in plasma in fig. 2.5. The current collection is described by the equations for a cylindrical probe given in tables 2.3 and 2.4.

We can notice from the simulation results that the total current in the case of a varying work function is subjected to the averaging effect around the plasma potential. This behavior has been quoted in literature as smoothening of the knee [2]. The flattening of the probe characteristics has been explained to be due to the electron energy smearing around the plasma potential, which is caused by different areas of the probes being charged to different potentials. We can see from fig. 2.5 that around the transition region of electron retardation to saturation region, some of the areas are still operating as retardation regions while the others have achieved positive attractive voltages. This leads the overall current across the probe to be averaged out across the lower and higher work functions leading to the absence of a sharp inflection point as predicted by the conventional model.

The incorrect identification of the inflection point would lead to an earlier prediction of the plasma potential which in-turn underestimates the electron density calculations. The work function variation also distorts the slope of the electron retardation region leading to

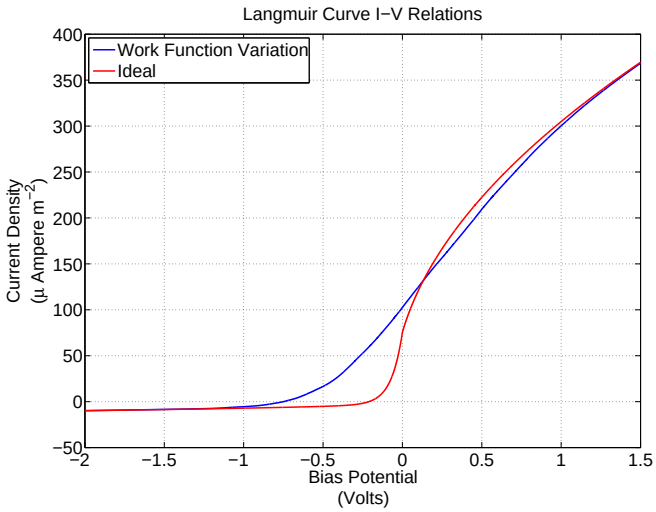

Fig. 2.5: Langmuir curve I-V relations.

misconstrued temperature measurements.

We compare the I-V curves generated by the work function variation model for all the three geometries with those defined by the traditional OML theory. Choosing a suitable ionosphere F region parameter set, temperature=800 Kelvin; density=1.1e10; plasma potential=0.8Volts; variance=0.2. The results are illustrated in fig. 2.6 and fig. 2.7.

As seen from the comparison figures, the deviation in the Langmuir probe I-V curve from the traditional OML theory-based ideal case to that of a work function variation model is pronounced for all three geometries especially in the flat plate and cylindrical collector. Spherical collector is relatively smooth due to inherently smooth plasma potential transition region. We use the model derived in this section to analyze the data from a sounding rocket mission which had a contaminated probe surface necessitating the use of structural non-uniformity factor to define the probe to plasma potential. The data quality and reliability is examined in the next section followed by the application of model for plasma analysis in the chapter following that.

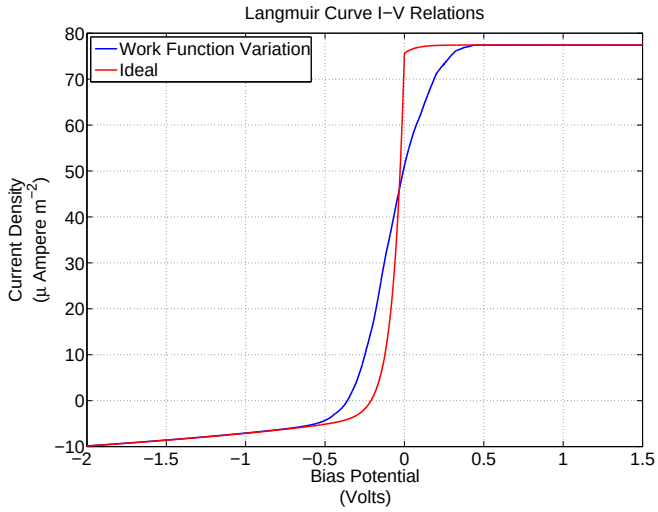

Fig. 2.6: Work function variation vs. ideal case: Flat plate geometry.

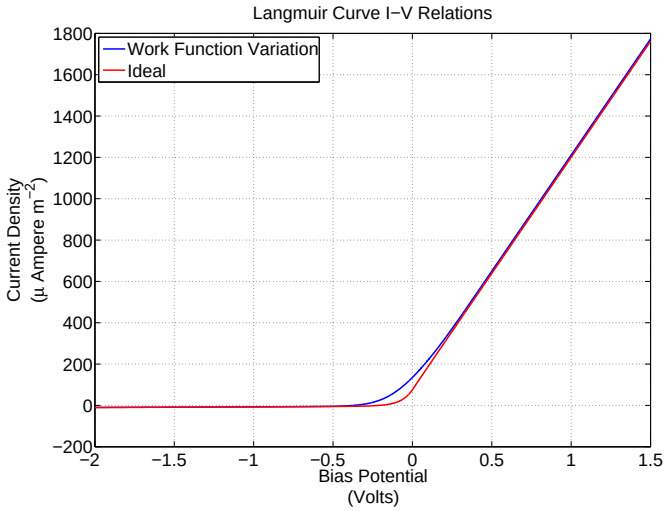

Fig. 2.7: Work function variation vs. ideal case: Spherical geometry.

Chapter 3

STORMS Mission

The scientific instruments onboard the STORMS Mission were built by University of Texas, Dallas and Utah State University/Space Dynamics Laboratory. The daughter payload, shown in fig. 3.1, designed by the Utah State University included a suite of instruments to measure relative and absolute electron density, electron-neutral collision frequency, temperature, and electric fields. The instruments were: Plasma Frequency Probe (PFP), Swept Impedance Probe (SIP), and DC Langmuir Probe (DCP) sensors, collectively called the Plasma Impedance probe (PIP) located on the fore direction of the rocket. The Sweeping Langmuir Probe (SLP) sensor was located in the aft direction of the rocket and the Floating Potential Probe (FPP) sensors are the four probes that are located perpendicular to the rocket spin axis and separated from each other by 90°. We present a brief overview of the USU instruments in the remainder of this section. The design and calibration efforts could be found in the following references: [31] and [32]. The details of the UTD payload and the science investigations of the mission can be found in the paper by Earle et al. [29].

The Sweeping Langmuir Probe makes measurements at both fixed voltages and ocassionally over a range of voltages. The probe was held constant at 3 volts and swept at every 20 seconds after 170 seconds of flight time. The sweep was from -1 to 3 volts. Thus periodic temperature and density measurements were made. Figure 3.2 shows the SLP raw data and fig. 3.3 shows the rocket trajectory with SLP sweep interval points. Temperature observations were made over the range of 270 to 390 Km. The fixed bias DC probe was held constant at -7 volts operating in the ion saturation region providing relative ion density measurements.

The floating potential probe implementation was a 0.1016 meters diameter, titanium nitrite coated; conducting sphere mounted approximately 0.0762 meters from the end of

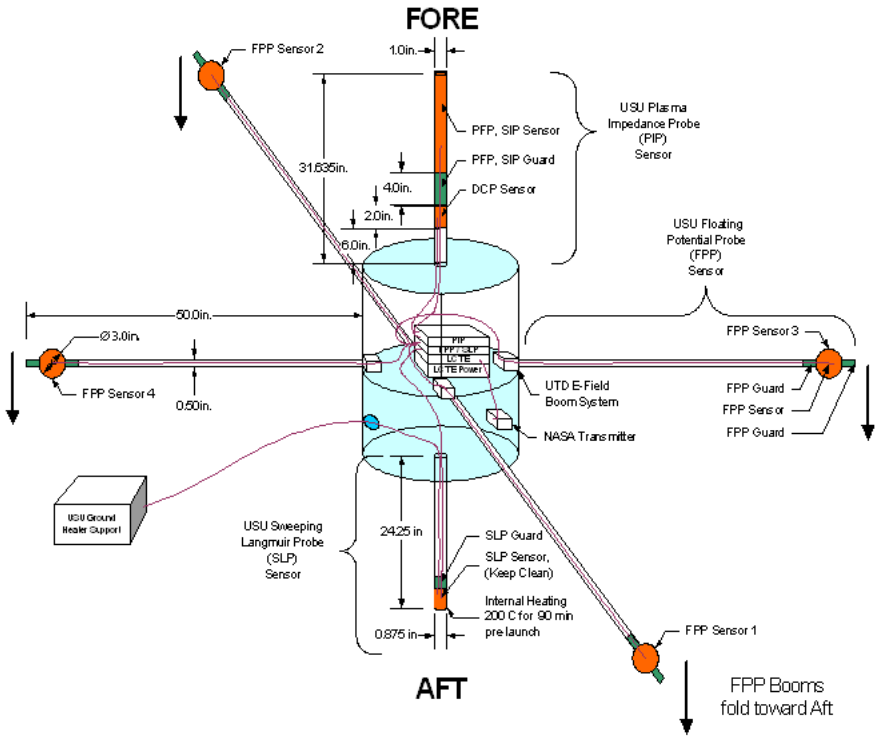

Fig. 3.1: Daughter payload onboard STORMS.

each boom. Each boom is 1.02 meters long and when deployed, the four FPP booms are perpendicular to the spin axis of the payload and separated by 90 degrees. This separates each sensor by approximately 2.032 meters from the next one and by approximately 2.794 meters from the opposing one. The FPP onboard this mission was implemented with a slightly different approach inorder to be able to measure the floating potential of the payload in addition to the electric field. Instead of measuring the voltage difference between two identical probes, the voltage difference between each probe and the payload skin is differenced through a difference amplifier and then digitized. The digitized readings from two oppositely placed probes could then be differenced to give the electric field measurements.

They make absolute density measurements by tracking resonance of the antenna at the various characteristic frequencies of the plasma. This technique has a distinct advantage of being independent of probe surface conditions, vehicle self-charging conditions, magnetic field, electron temperature, etc., as well as providing fine resolution of density measurements.

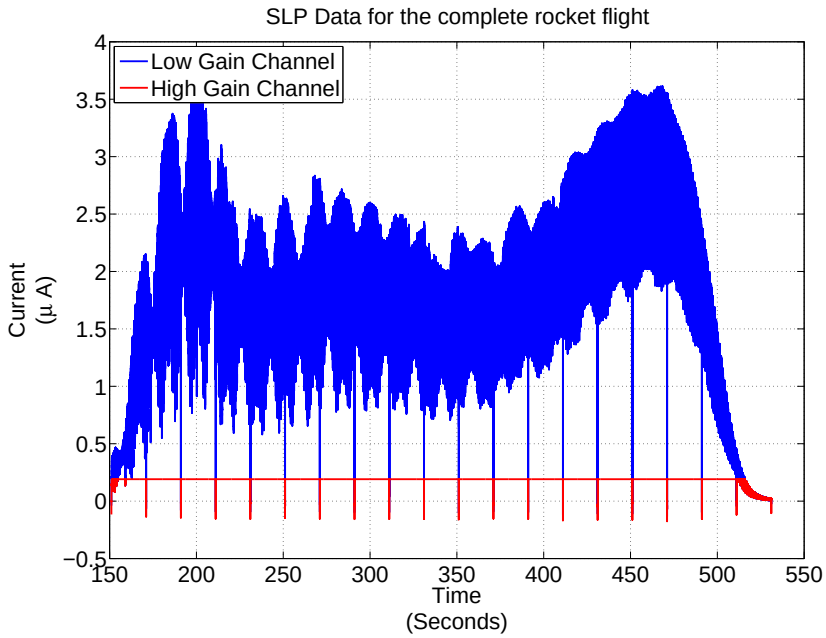

Fig. 3.2: Raw data of SLP sweeps.

The Plasma Frequency Probe (PFP) tracks the upper hybrid frequency, and the absolute electron density could be derived from this measurement. In the Sweeping Impedance Probe (SIP) technique, the instrument is swept over a range of frequencies and the antenna impedance is measured. The electron density can be obtained by matching the measured impedance curves against the impedance probe theories. The PFP instrument onboard the STORMS mission did not successfully track the upper hybrid frequency, and hence no reliable measurements were available. However the SIP, which was swept from 0.1-20 MHz, provided valuable set of data to study the density fluctuations and structures. The SIP antenna made 128 point measurements between the set frequency ranges of the impedance magnitude.

3.1 PCM Telemetry Format Description

The telemetry requirements are determined by the science question that the mission is launched to address. In the case of STORMS, the spatial resolution for making measurements was determined to be between 0.1 to 100 meters depending on the instrument.

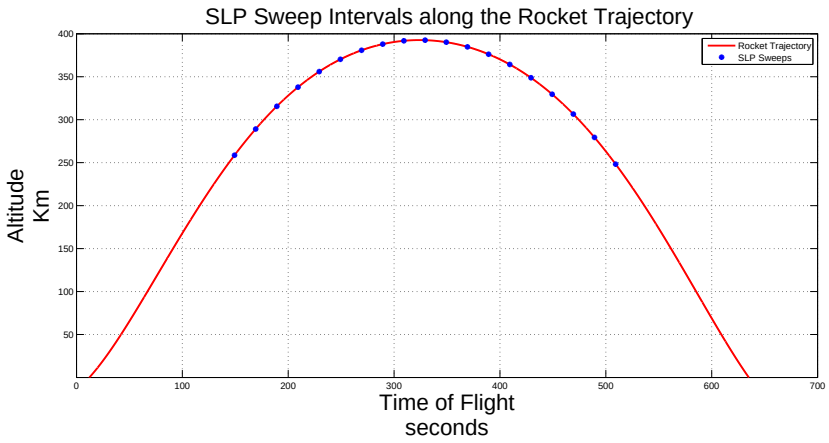

Fig. 3.3: Rocket trajectory with SLP sweep points.

Figure 3.4 has the data sampling rate of all the instruments onboard the STORMS daughter payload. The data from the PCM matrix is extracted and converted from counts to the respective measurements units using the calibration constants. These measurements are then investigated for usability in the next section. The telemetry matrix is found in Appendix A.

3.2 Data Quality Analysis

The data from SLP for a single sweep at an altitude of 350 Km is presented in fig. 3.5. The corresponding data from the floating potential probes and the sweeping impedance probes is presented in the fig. 3.6. The data from all the instruments exhibit a periodic noise in their measurements. This noise, upon investigation, was found to be correlated with the SIP. It was observed that at low driving frequencies of the SIP instrument, the SIP, FPP, and the SLP measurements were corrupted. The noise was correlated with the frequency on the SIP. When the driving frequency was near or below the local plasma frequency and the electron gyro frequency, the potential of the whole payload relative to the plasma was affected. This case of low frequency condition of RF plasma sheaths influencing spacecraft potential and payload measurements is often referred to as “sheath-rectification.” Though the electrodynamics of the spacecraft charging process due to RF driven plasma

Channel	Label	Sample Rate (Hz)	Word Size (Bits)	Words/ Sample	Bit Rate (Bits/s)	Word Rate (Word/s)
DCP Low Gain	DCPL	2441.4	16	1	39062.5	2441.4
DCP High Gain	DCPH	2441.4	16	1	39062.5	2441.4
PFP Low Bits	PFPH	2441.4	16	1	39062.5	2441.4
PFP High Bits	PFPL	2441.4	16	1	39062.5	2441.4
SIP Impedance Magnitude	SIPM	76.3	16	128	156250.0	9765.6
SIP Impedance Real Total	SIPR	76.3	16	128	156250.0	9765.6
SIP Impedance Imaginary Total	SIPI	76.3	16	128	156250.0	9765.6
SIP Impedance Real Delta	SIPRD	76.3	16	128	156250.0	9765.6
SIP Impedance Imaginary Delta	SIPID	76.3	16	128	156250.0	9765.6
SIP Free Space Capacitance	Co	76.3	16	1	1220.7	76.3
PIP Housekeeping	PIP	76.3	16	16	19531.3	1220.7
SLP High Gain	HG	38.1	16	512	312500.0	19531.3
SLP Low Gain	LG	38.1	16	512	312500.0	19531.3
FPP Sensor 1	VS1	4882.8	16	1	78125.0	4882.8
FPP Sensor 2	VS2	4882.8	16	1	78125.0	4882.8
FPP Sensor 3	VS3	4882.8	16	1	78125.0	4882.8
FPP Sensor 4	VS4	4882.8	16	1	78125.0	4882.8
FPP Least Significant Bits	Vlsb	4882.8	16	1	78125.0	4882.8
SLP/FPP Housekeeping	SLP	76.3	16	15	18310.5	1144.4
NASA GPS	GPS	4882.8	16	1	78125.0	4882.8
NASA Magnetometer	A2, A3, A4	1220.7	16	3	58593.8	3662.1
NASA Housekeeping	Axx	152.6	16	24	58593.8	3662.1
NASA Time Event	T1A, T2A	152.6	16	2	4882.8	305.2
Spare	Spare	4577.6	16	1	73242.2	4577.6
TM Overhead	SFID, SYNC	14648.4	16	1	234375.0	14648.4
				Total	2,500,000.0	156,250.0

Fig. 3.4: Sampling rate of instruments onboard STORMS daughter payload.

sheath modifications is not completely quantified, studies on the Oedipus-C mission floating voltages and also ISIS II [33] and Cosmos 1809 observations [34] have discussed the physical process causing the induction of harmonic components in the current collection process defining the floating potential voltages in RF driven plasma sheaths. Further information on the physical process of this regime of plasmas can be found in the references cited above and the referrences within.

We can also see from the figure that the FPP measurements are being subjected to a rise in the region corresponding to electron collection region of the SLP. The payload charges more negative, relative to the plasma resulting in general decreased collection by the Langmuir probe and the enhanced observations of the floating potential on the FPP sensors. This can be clearly seen in fig. 3.6. This behavior is an indication of spacecraft

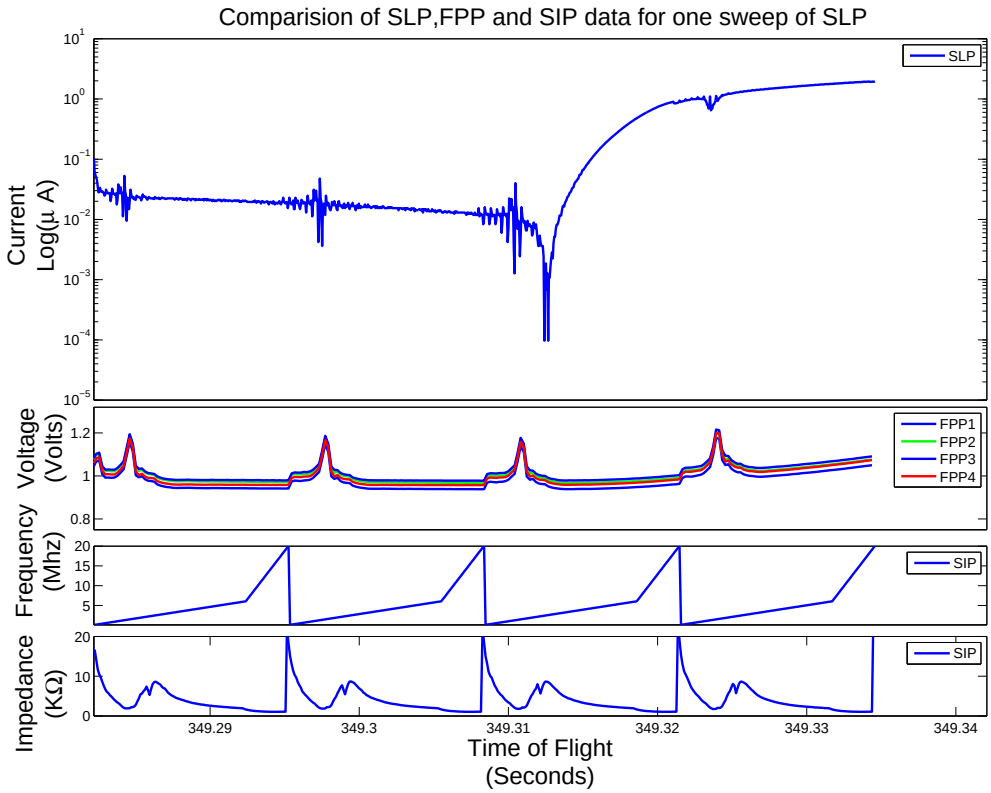

Fig. 3.5: Data comparison of daughter payload for one SLP sweep interval.

self-charging effect. The FPP measurements are the payload potential pointers. This rise in the electron collection dominant region is a consequence of the payload potential being swung around by SLP due to the small surface area ratio of spacecraft to the probe. The spacecraft, the probe, and the surrounding plasma form a closed loop system and when the probe is drawing in electrons (fig. 3.7), the spacecraft body needs to collect ions. Ions being massive and slower would be collected in fewer numbers and require a sufficiently large collecting area to balance out probe electron collection. Experimentally, the ratio of spacecraft to the probe has been established to be around 1000. But in the case of STORMS sounding rockets, this area was found to be around 250. Inorder to maintain a balance, the spacecraft ground shifts negative to reduce the electron collection by the SLP. It can be seen from fig. 3.6 that the FPP readings which give the payload potential (spacecraft ground) are rising (spacecraft reference ground becomes more negative) as the SLP sweep

becomes more and more electron-collection-dominant.

The SLP was being swept every 20 second on reaching an altitude of 270Km up-leg and was operated in this mode till the rocket reached 270Km on the down-leg. This provided 19 sweeps of the SLP in this interval which can be seen in fig. 3.3. The SLP data before being subjected to data analysis needs to be filtered out to remove the SIP induced periodic noise. This limited the number of points in each sweep available for the data analysis. It was found that the number of points suitable for curve-fitting was half the actual measurements made.

It was also observed that some of the sweeps were affected by the SIP noise at the transition regions leading to significant loss of useful data. This made them unsuitable for the single-stage curve-fitting process (which will be discussed in the Chapter 4) used in the plasma analysis. This curve fit is dependent on the transition region indicators namely the floating potential and the plasma potential. Absence of quality data about either of these points would render the data unsuitable for analysis. (Details of the curve fit procedure is explained in Chapter 4). The same holds good for the multi-step procedure of iterative curve-fitting [24], as well as the traditional method of graphical analysis [35]. Both of these methods require the transition points to be known with great precision to deduce density and temperature of the charge carriers.

Some of the sweeps analogous to the sweep, seen in fig. 3.8, were noisy in the area around floating potential and post-filtering, lose the entire region making them rather discontinuous around floating potential, and hence not data-analysis-suitable. It was also seen that some of the curves similar to the one seen in fig. 3.9 were subjected to additional noise in electron saturation region. This led to the entire electron saturation region data being noisy. Quality data points were lost on filtering and hence such sweeps were again not fit for the plasma analysis. Hence, it was seen that only the data between 270 to 390 Km up-leg and 390 to 320 Km down-leg was suitable for SLP based data analysis. (Appendix B has the plots for all the 19 sweeps.)

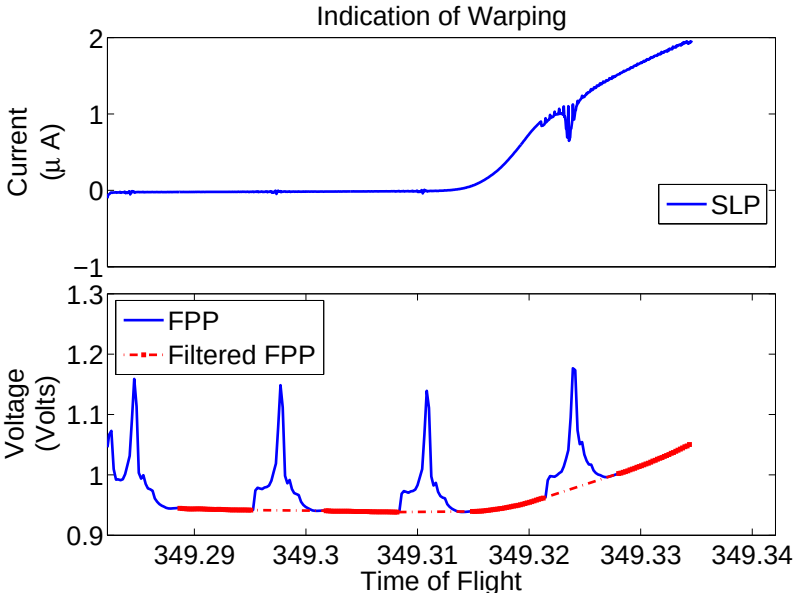

Fig. 3.6: FPP and SLP data to illustrate the surface area ratio effects.

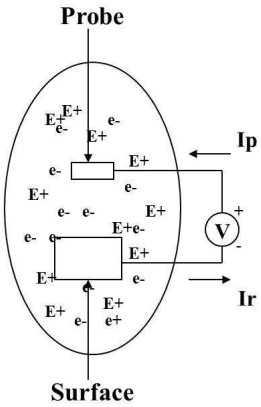

Fig. 3.7: SLP-spacecraft-plasma current collection dynamics.

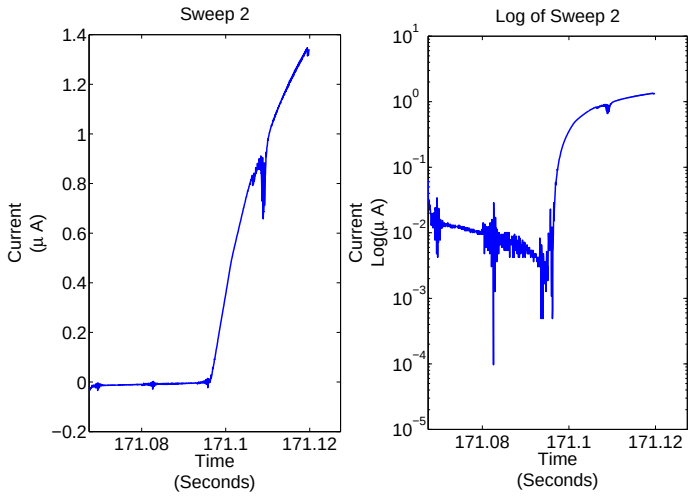

Fig. 3.8: Langmuir probe data with noisy transition region: Floating potential region.

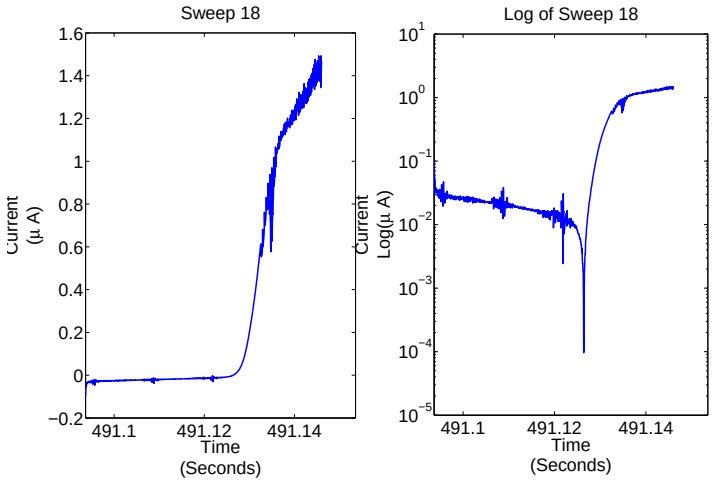

Fig. 3.9: Langmuir probe data with noisy transition region: Plasma potential region.

Chapter 4

Data Analysis

The first step in analyzing the Langmuir probe data is to define the plasma regime under study. The ionosphere at the F region could be best described as low-pressure plasma with a Maxwellian distribution of velocities. The Debye sphere radius would be of the order of a few centimeters, which would not add any significant perturbations caused by the magnetic field of the Earth. Being a night time mission, additional sources of current collection like secondary emissions and photocurrents do not affect the current collection dynamics. Hence, the data collected could be best summarized as non-magnetic, collision-less, and Maxwellian under Mesothermal conditions.

4.1 Techniques of Data Analysis

On establishing the plasma regime, the data could be analyzed to infer the plasma properties using the suitable current collection equations. The traditional approach of extracting the plasma behavior using the current collection equations is to use the method of graphical analysis of the I-V curve. This method involves deducing the logarithmic-slope of the electron current vs. voltage curve to estimate the electron temperature. A straight-line fit to the electron retardation region and electron saturation region is done. The point of intersection of these two gives the plasma potential. The electron saturation current at plasma potential is used to deduce the density from the already estimated temperature. The accuracy is estimated to be within 25 mV of the plasma potential and 10 kelvin of electron temperature. However, for some of the ionosphere studies, accuracy to the order of 5% or more is desired for temperature and density gradient measurements. Hence, more precise methods of data deductions are required to better estimate the plasma behavior.

Alternative approach used to study the Langmuir probe data is to use regression analysis techniques. Here suitable current models for the plasma regime under study are fit with the collected data in a least-square-sense to estimate the plasma properties. This process could be represented as

$$\begin{aligned} &min_{fitvariables} \left\| F\left(\text{fit variables,applied voltage}\right) - \text{Measured Current} \right\|_2^2 = \\ &min_{fitvariables} \sum_i \left(F\left(\text{fit variables,applied voltage}\right) - \text{Measured Current} \right)^2 . \end{aligned} \tag{4.1}$$

The $F(fitvariables, appliedvoltage)$ term in the equation is the current collection model generated value of current, which will be matched with the measured current by adjusting the fit-variables. These fit-variables are the co-efficients of the nonlinear current collection equation. The fit variables are chosen to be the plasma properties and parameters influencing the probe current collection behavior. These variables are processed through the regression analysis techniques to minimize the difference between the model-generated data and measured data.

In this method, a first guess of the plasma properties are made using the graphical method of I-V curve analysis. These parameters are further refined by least square curve-fit of the data to the current model [36]. The least square fitting is first done for the data set around the floating potential to determine the temperature. Once the electron temperature is determined; the data set around the plasma potential is fit in a least-square sense to determine the plasma density. The curve-fit is done separately for the two regions because of the difference in the magnitude of the current in the two transition regions. Being of higher magnitude, the region around the plasma potential (density) would get more weightage in the least square fit calculation, leading to a poor fit in the retardation region (temperature). By fitting separately, difference in the weights of the two regions would not hamper the accuracy of the measurement. However, due the curve being subjected to fitting of only a selective data-set, we have to perform multiple iterations to choose the data-set leading to the best fit.

The regression analysis technique apart from being more accurate is also useful in

understanding the behavior of the various parameters influencing the current collection. Behavior of effective area of collection, velocity distribution, etc., could be studied by setting these collection parameters as tuning variables for the regression analysis. Owing to these advantages, we have chosen the regression analysis technique of fitting the model to the data in order to study the plasma parameters.

The fit variables used to perform regression analysis are density, temperature, and effective probe-to-plasma potential. The effective probe-to-plasma potential is in-turn expressed as a factor of two variables, namely, plasma potential and the geometry factor of the probe. The geometry factor of the probe determines the effective probe area of charge carrier interaction. The equations are formulated assuming that the area of collection is known. But this does not hold well in the case of wake region current collection. The charge carriers in the wake region are rarified leading to the effective area of the probe behaving as a cylindrical collector to be undefined. Hence, the geometry factor of the probe is set as a fitting parameter instead of being fixed at 0.5.

Also, the surface structure non-uniformity induced probe-to-plasma potential variation is an unknown parameter for the STORMS data. Hence, we introduce a third variable, namely the variance of the probe surface work function to deduce the effective probe to plasma potential. The variation of the work function quantifies the measure of surface non-uniformity. The variance of the work function is a factor influencing the entire I-V curve behavior unlike other variables, whose influence could be isolated to specific regions of the I-V curve. Hence, selective data-fitting would not be feasible. This means we need to circumvent the problem of difference in weights of the different regions.

We have therefore, used the method of normalizing the measured data by the current collection model generated data. This method of taking the ratios would lead the curve-fit to be done with equal weights at all the regions of the I-V curve. The least square analysis involves doing a regression analysis of the ratio vs. unit vector by finding the best value of

the fit parameters or the variables.

$$min_{fitvariables} \left\| \frac{F\,(\text{fit variables,applied voltage})}{\text{Measured Current}} - \text{Unit Vector} \right\|_2^2 = min_{fitvariables} \sum_i \left(\left(\frac{F\,(\text{fit variables,applied voltage})}{\text{Measured Current}} \right) - \text{Unit Vector} \right)^2 \tag{4.2}$$

The fit variables considered in our case are:

Density (N_e),

Temperature (T_e),

Plasma Potential (ϕ_p),

Standard Deviation of the work function (σ),

Geometry Factor (β).

4.2 Data Analysis Results

We have used the "lsqcurvefit" algorithm which is an inbuilt MATLAB function. The least square fit of data is done for all the sweeps whose data quality was established to be good. The results are presented in logarithmic plots. The goodness of the fit for the ion current cannot be established in a normal I-V curve due to the ion current getting masked by the electron current magnitude. A logarithmic plot would ensure that the ion collection regions are well defined and also the goodness of the fit can be easily established.

The equations for ions and electrons defined in Chapter 2 in table 2.3 and table 2.4 are used to describe the model current which is tuned using the five fit variables defined in previous section to analyze the data. As described in Chapter 3, we have discarded the noisy data points, subtracted the FPP voltages to account for surface area ratio effects before we perform regression analysis.

We present the results of doing the curve-fit employing the work function theory by means of altitude-density and altitude-temperature plots. The altitude plots are available for only limited range for both the upleg and downleg of the flight due to reasons established in Chapter 3. Before that, we present the results of the curve-fit done using the work function

variation theory.

4.2.1 Surface Morphology Effects

Figure 4.1 presents the results of curvefitting done using work function variation theory. The fitting results for the remaining of the SLP I-V curves are presented in the later section. We first present the results of comparison of using work function theory vs. an OML theory based current model for the moving probe. This is done to illustrate the importance of incorporating the surface structure effects. Note that the reference potential effects or the warping effects have been accounted for. The fit around the floating and plasma potential for am OML current equation trial, as seen in fig. 4.2, is found to be poor. A sharp inflection point is predicted for an OML theory-based model as earlier explained in Chapter 2. The data is smoother around the plasma potential and the smoothening-effect due to averaging of the various non-uniform regions of collection embedded into the work-function-variation theory makes an excellent fit.

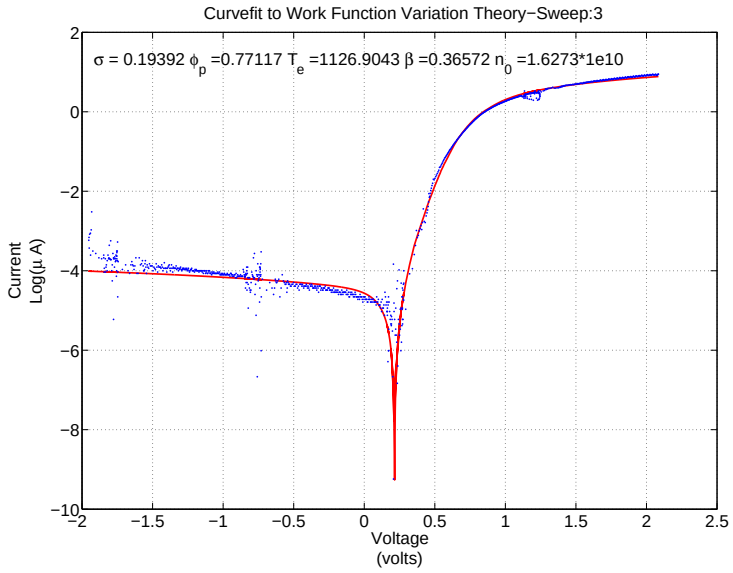

Fig. 4.1: Curvefit to STORMS data using work function variation theory.

The curve-fit results to illustrate the importance of considering the effects of small area ratio of the spacecraft to probe surface is shown in fig. 4.3. We can see from fig. 4.2, the importance of identifying the correct probe-plasma potential. An absence of the floating-potential-shift compensation leads to an incorrect identification of the floating point. This in-turn translates to an incorrect identification of temperature.

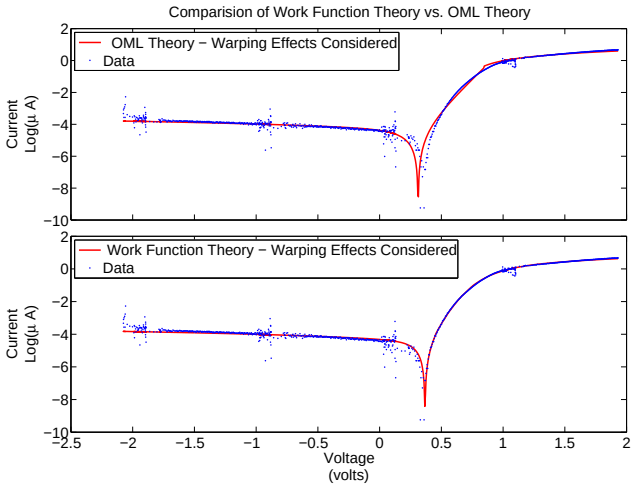

Fig. 4.2: Curvefit to work function variation theory and OML theory of current collection.

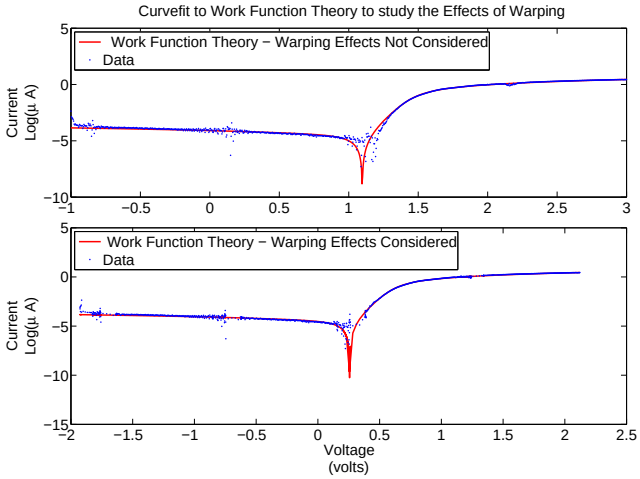

Fig. 4.3: Illustration of surface area ratio effects.

We present the profiles for density and temperature calculated using both OML and work-function-variation theory. Note that the profiles created here are used to illustrate the disparity in measurements and not to describe the ionosphere state. These figures are snapshots of the rocket measurements at different rocket wake structure and coning conditions. The density measurements are affected by these two factors. Hence to create an altitude profile of density, we need to consider only those measurements taken at particular orientation of the rocket. Such a profile is defined later in this chapter.

We can see from fig. 4.4 and fig. 4.5 that not accounting for the non-uniform surface behavior results in higher temperature and lower density calculations. The lack of embedding work function variation effects leads to an earlier identification of transition regions. An earlier identification of floating potential would mean that the electron energy is estimated to be higher than in actuality, leading to a higher temperature deduction. Similarly, the premature-identification of the plasma potential translates into the random current to be of lower magnitude or due to lesser number of electrons.

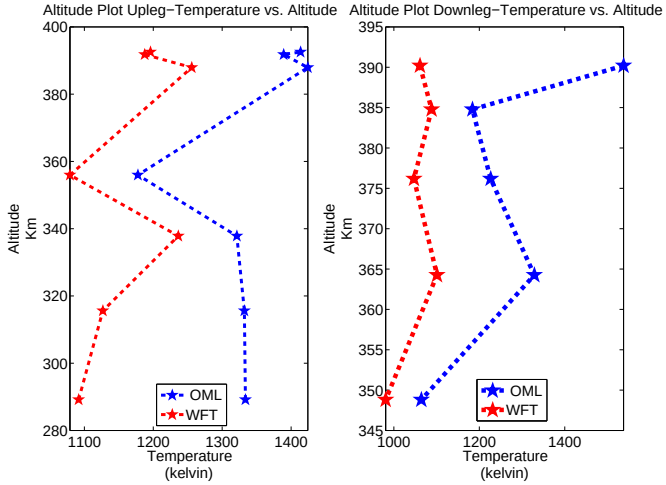

Fig. 4.4: Surface morphology effects on temperature deductions.

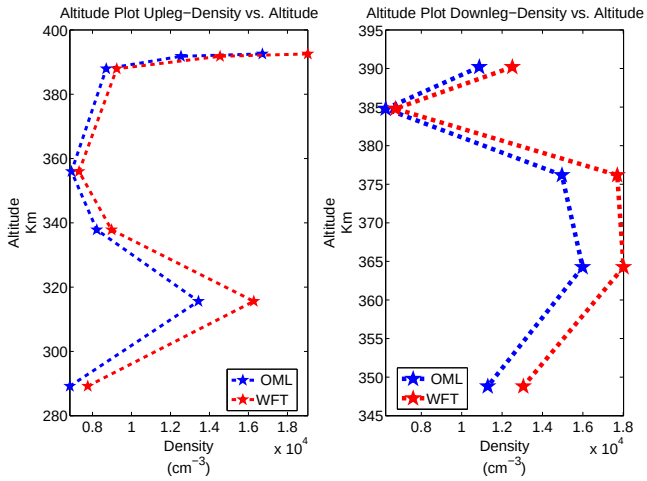

Fig. 4.5: Surface morphology effects on density deductions.

4.2.2 Inclusive Effects of Probe and Plasma Conditions on Data Analysis

One of the interesting observations in this data analysis was the behavior of the least-square-fit algorithm. We are tuning five different variables to analyze the data in accordance with the model. Use of multiple tuning variables has been often associated with introducing extreme flexibility and bending the model in non-physical ways to fit the data. If this indeed would be true, the model would have fit the data even when the effects of warping or work-function-variation were ignored. But it was shown that the algorithm does not behave well when these effects are ignored. Hence, the data-model matching technique proves to work well. We use another example to illustrate this point. We do another trial of fitting the data to the model, but without considering the ion-ram effects.

The comparison of fitting the data to the model with and without the ion ram current is presented in fig. 4.6. We can see from fig. 4.6 that the ion ram current effects in the model would cause the model vs. data to not fit well in the ion saturation region and this gets translated into other regions of operation as well. This indicates that embedding all the plasma and probe effects into the current model is essential for an accurate plasma analysis.

We can see from fig. 4.7 that a varying β model better describes the electron saturation

region collection. A fixed β of 0.5 as described by theories of current collection does not seem to hold good when applied to the data. This illustrates the possibility of wake effects and other practical constraints of achieving an ideal cylindrical collecting area when the probe is in flight.

The fact that a comprehensive outlook on all probe and plasma conditions is essential to perform accurate plasma analysis is illustrated from the results of data analysis presented here. The success of single-stage fitting is another indicator of the importance of the inclusive effects of the probe and plasma behavior on the current collection process.

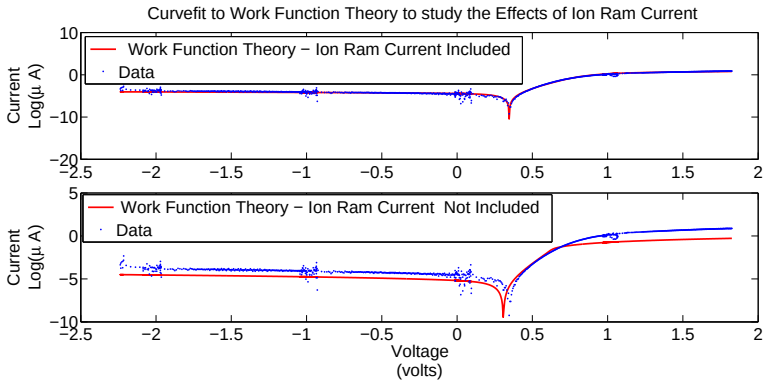

Fig. 4.6: Ion ram current effects.

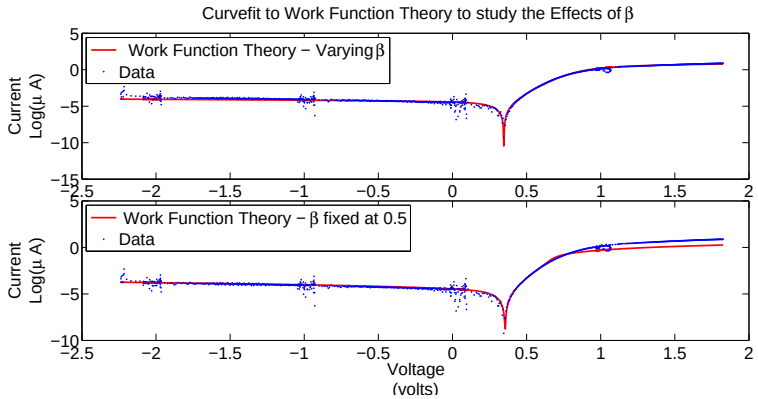

Fig. 4.7: β effects.

4.2.3 Work Function Variation Theory Results

In this section, we present the results of the work-function-variation theory analysis using the quality data points of the SLP, which were identified to be suitable for the plasma analysis. The curvefit of each of the individual sweeps are presented later in this section.

It was found that the standard deviation varies between 0.1 to 0.18 volts. The model is defined to have a zero mean which means that the work function spread is up to about 0.18 volts across the probe surface for the flight. The work function variation of TiN coating was experimentally studied to be around 0.0015 eV [13]. Also, the work function was found to be time invariant. The study of the variation of the work function across the probe surface indicates clearly the non-homogeneity of the surface properties. A variation of upto 0.18 eV shows that the work function is not due to the inbuilt lattice structures. Similarly, the time variation of the work function indicates an external trigger to this event.

We also observe that the geometry factor is not constant but varies considerably indicating that the collection area in the saturation regions is not a constant across the probe and the wake effects need to be considered. A plot of σ and β variation with flight are presented in fig. 4.8 and fig. 4.9.

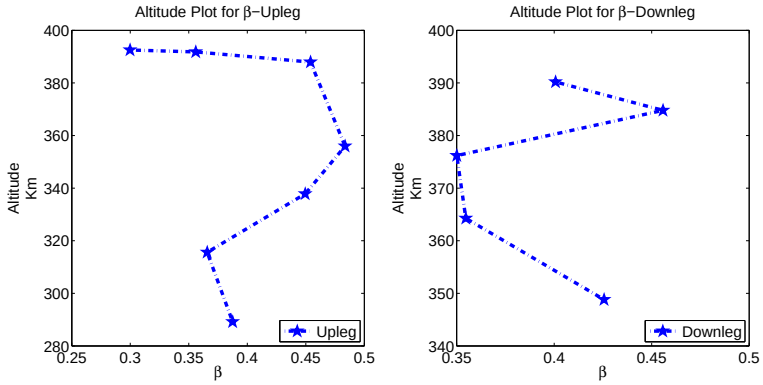

Fig. 4.8: β-altitude profile.

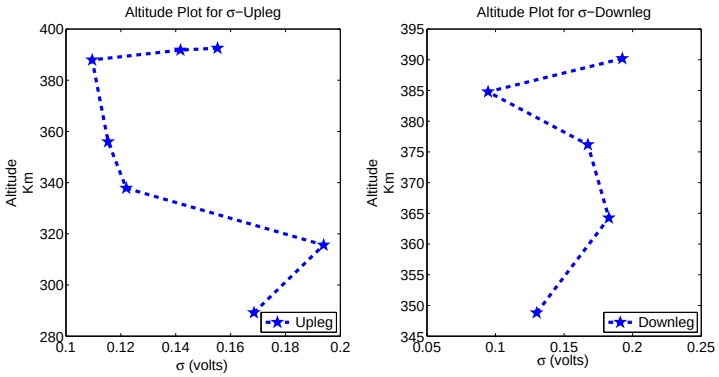

Fig. 4.9: σ-altitude profile.

In this chapter we saw the suitability of using our work-function-variation model for analyzing the Langmuir probe data subjected to surface non-uniformity. As stated earlier, another aspect of the surface property, which is instrumental in successful measurement, is the size of the probe. It was seen during the data analysis that an insufficient probe area would lead to a shifting floating potential. This problem would be magnified several times when we put a Langmuir probe on a CubeSat. We investigate this problem in the next chapter and present our findings. Next, we present the results for all the data-analysis-suitable SLP sweeps in fig. 4.10, fig. 4.11, and fig. 4.12.

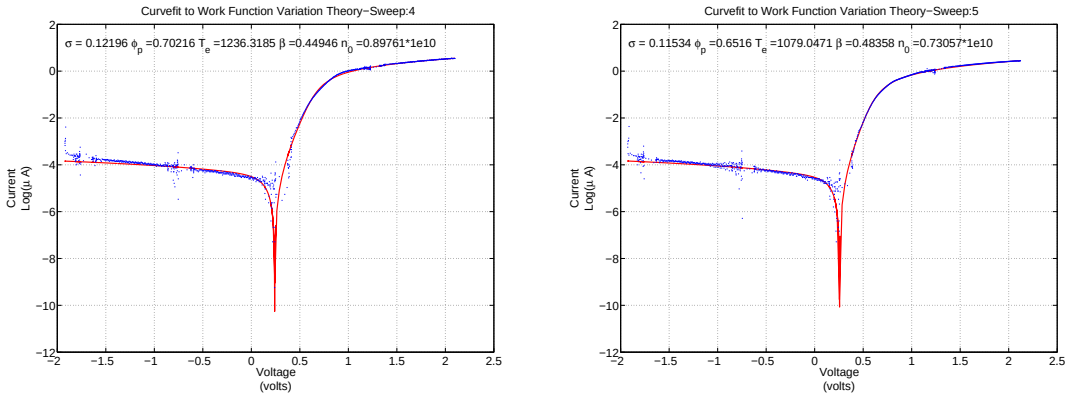

(a) Sweep4 (b) Sweep5

Fig. 4.10: Curvefit results of sweeps 4 and 5.

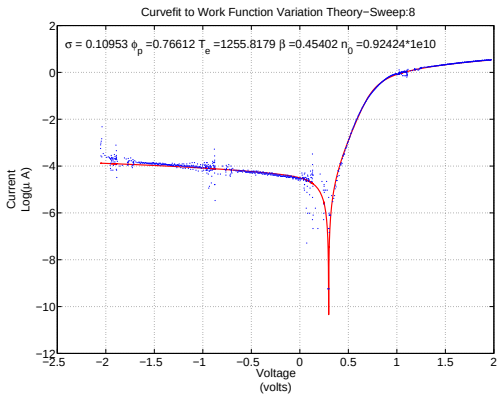

(a) Sweep8

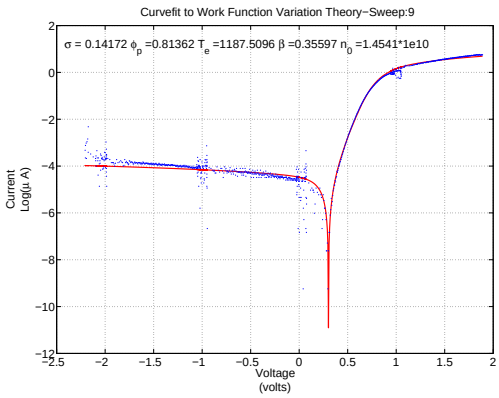

(b) Sweep9

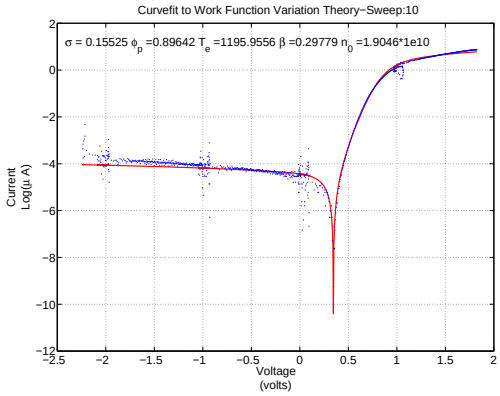

(c) Sweep10

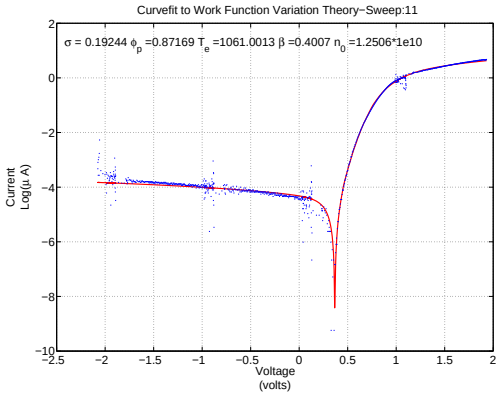

(d) Sweep11

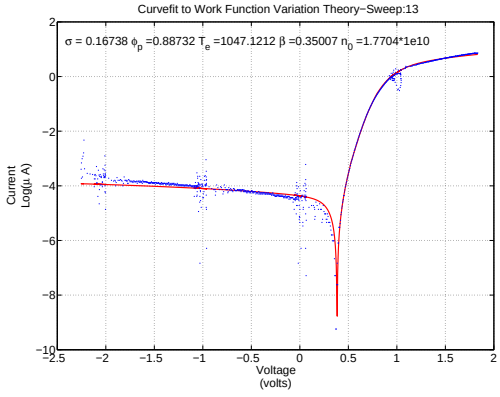

(e) Sweep13

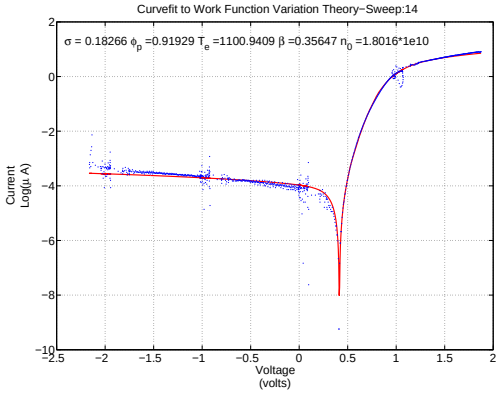

(f) Sweep14

Fig. 4.11: Curvefit results of sweeps 8 to 11 and sweeps 4 to 15.

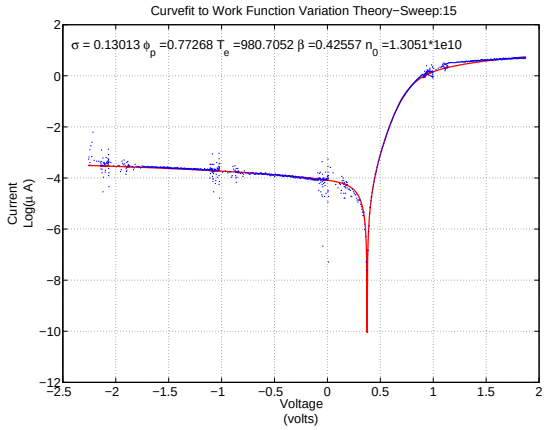

(a) Sweep15

Fig. 4.12: Curvefit result of sweep 15.

4.3 STORMS Density Data

The SLP probe data measurements were subjected to periodic spin modulations due to the coning of the rocket. The plot of upleg measurements corresponding to the sweeping mode and the fixed mode are plotted in fig. 4.13 (a). The effect of the rocket spin angle and coning is illustrated in fig. 4.13 (b), which is a snapshot of the downleg measurements. Deducing the accurate density profile would require us to find the precise value of the spacecraft spin angle and also the effect of coning. This is beyond the scope of this work. However for the sake of completeness, we have presented the density profiles deduced by the DC probe to illustrate the density profiles.

The DC probe which was fixed at -7 volts could be used to deduce density measurements. Figure 4.14 (a) and fig. 4.14 (b) have the DCP current data plotted against the time of flight and altitude. The data below 200Km was found to be not reliable due to low signal strength. We only use the data beyond this point to deduce density. The DCP density values need to be calibrated in order to compute absolute density [37]. The SIP makes absolute measurements of plasma density. We compute the density from SIP for a particular altitude and normalize the DCP data to plot the density-altitude profile for the DCP flight data. The SIP data is analyzed using Balmain's theory to compute the plasma

frequency which in-turn gives us the density [38]. The SIP data chosen is at an altitude about 310 Km as shown in fig. 4.15 (a). Data from IRI model and a digisonde present at Wallops Island has been used to fill-in the gap below 200 Km [29] as seen in fig. 4.15 (b).

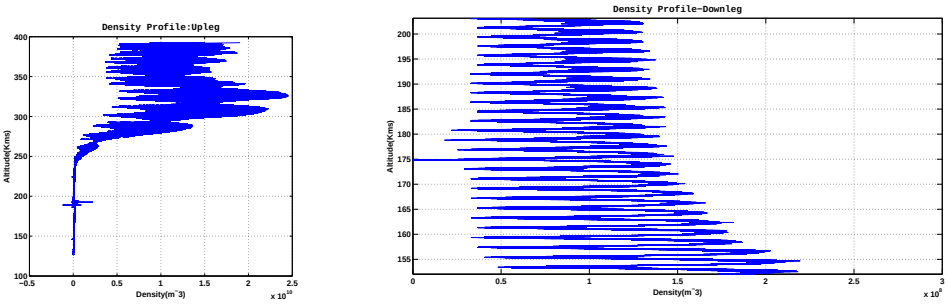

(a) SLP Density-Altitude Profile

(b) Illustration of spacecraft spin effects

Fig. 4.13: STORMS density data presentation.

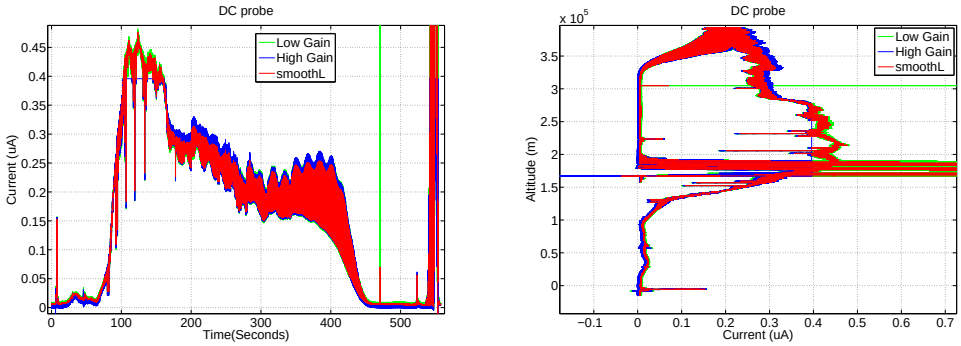

(a) DCP Current Plot

(b) DCP data altitude plot

Fig. 4.14: STORMS DCP data.

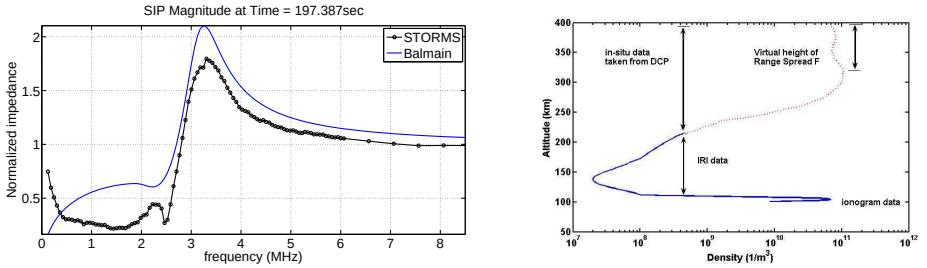

(a) SIP data vs. Balmain's theory (b) DCP data normalized using SIP

Fig. 4.15: DCP density deductions.

Chapter 5

Surface Area Implication for Langmuir Probe Measurements on CubeSats

CubeSat regimes are increasingly becoming the most popular form of space measurement platform currently with their promise to make scientific experiments in space cheaper. Langmuir probe due to their versatility in making measurements in a wide variety of space environments would be the one of the most ideal candidates for CubeSat missions. Putting Langmuir probes on constellation missions to make spatially and temporally resolved measurements with great precision and resolution would be highly beneficial for understanding the space environment.

The Utah State University/SDL is part of a multi-university tie-up to investigate space weather phenomenon for a NSF CubeSat mission named- Dynamic Ionospheric CubeSat Explorer, which is referred to as the DICE mission [39, 40]. This mission has Langmuir probes for studying the plasma behavior. CubeSats with their very limited surface area would pose a challenge to make accurate scientific measurements from a Langmuir probe. We investigate the expected measurements from the probe on this form-factor using a SPICE Model to inspect the current collection process.

5.1 DICE Mission Analysis

DICE was selected and funded by the National Science Foundation in October 2009 in response to a cooperative proposal from the Utah State University/Space Dynamics Laboratory (USU/SDL), ASTRA Inc., and Embry Riddle University. DICE is one of several missions currently in development under NSF's CubeSat-based Science Mission for Space Weather and Atmospheric Research program.

The DICE mission consists of two 1.5U CubeSats deployed simultaneously from a single

P-POD into the same orbit. Over time the satellites will, due to differences in the ejection velocity, separate relative to each other. The use of two identical satellites permits the deconvolution of spatial and temporal ambiguities in the observations of the ionosphere from a moving platform. The science objective of DICE is to understand the Storm Enhanced Density (SED) features which occur frequently in the US in the late afternoon during magnetic disturbances. The cause of this phenomenon is currently unknown, and is a topic of great scientific and practical interest. Ionospheric variability has a dramatic effect on radio frequency (RF) systems; for example, large gradients in ionospheric electron density can impact communications, surveillance, and navigation systems.

The DICE science objectives will be achieved via in-situ ionospheric electric field and plasma density measurements onboard the two spacecraft. These measurements will be made using two instruments: the Electric Field Probe (EFP) for electric field measurements and the fixed-bias DC Langmuir Probe (DCP) for ion density measurements.

Figure 5.1 illustrates the DICE spacecraft and instrumentation configuration and table 5.1 has the instrument configuration details. Each of the two DICE spacecraft is identical in design and function and conforms to a 1.5U CubeSat form factor (10x10x15 cm). The four EFP booms extend 5 metre each away from the spacecraft with spheres on the ends of the booms. The four shorter booms on the bottom-side of the spacecraft comprise the ultra-high frequency (UHF) communications turnstile antenna and are 0.2 m in length. The UHF booms also provide balance for the controlled spin of the spacecraft. The DCP sensor spheres are supported on the top and bottom of the spacecraft by extending scissor booms that extend 8 cm away from the spacecraft.

The electric field probe consists of DC field measurements, V12 and V34, a floating potential measurement, V1S, and a four channel spectrometer to examine wave power. The Langmuir probe is operated in either a fixed DC mode or a sweeping mode.

5.2 Surface Area Ratio Problem: Description of the Problem Statement

The biased probe, spacecraft, and the surrounding plasma constitute a closed-loop current collection system. When the probe is operating at positive voltage, the spacecraft

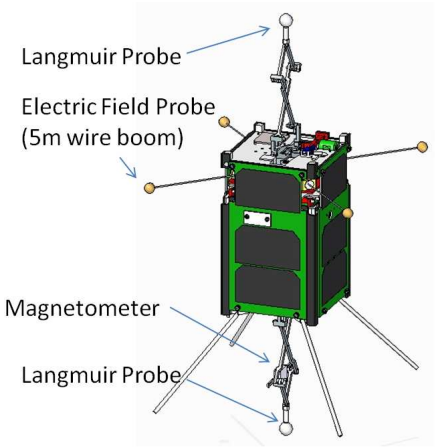

Fig. 5.1: The DICE spacecraft with electric field booms in partial deployment.

return current would be due to positive ions. Ion current is of significantly lower magnitude, and hence would require a large spacecraft surface to be available for collection to balance out the probe current due to electrons.

An absence of such a surface would swing the spacecraft ground more negative to compensate for the inability to collect sufficient ions. This shifts would in turn reduce the effective probe to plasma potential leading to decreased current collection at the probe. In the case of a fixed bias probe held positive, the shift in the ground could force the region of operation to transition from electron collection to retardation and finally ion saturation resulting is useless data.

The modeling efforts to study this problem are done using the NSF DICE CubeSat mission as the prototype. The CubeSat has a 10 cm x 10 cm x 15 cm form factor. It has two sweeping Langmuir probes (SLP) and four electric field probes (EFP). The SLP probes are 1.27 cm diameter spheres giving the effective area ratio with respect to the spacecraft range from 10 to 100 based on the surface materials on the CubeSat. The spacecraft has solar panels and such other non-conducting areas, and hence we need to model this into the model of current collection. We have modeled the worst-case scenario of having numerous non-conducting surfaces on the spacecraft surface. The various collecting areas for the probe and the CubeSat are expressed in table 5.2.

Table 5.1: DICE instruments.

Langmuir and Impedance Probe Option			
Instrumentation Techniques	Parameters	Rate	Science Performance
Electric Field Double Probe (EFP)	E	70 or 35 Hz	±0.1 to ± 200 mV/m 1%
Electric Field Spectrometer Ch 1: 16-32 Hz Ch 2: 32-64 Hz Ch 3: 64-128 Hz Ch 4: 128-512 Hz	E- PSD	1Hz	0.1μV/m to 1μV/m Integrated over spectral bands
Floating Potential Probe (FPP)	V_f	70 or 35 Hz 1/120 Hz	±0.1mV to ±8V
DC Langmuir Probe (DCP)	δN_e	70 or 35 Hz	$1000 - 10^8 cm^{-3}$ 5%
Sweeping Langmuir Probe (SLP)	δN_e δN_i T_e V_f V_p	1/120 Hz	$100 - 10^7 cm^{-3}$,5% $1000 - 10^8 cm^{-3}$ 500-5000K ±5mV to -4 to2V ±5mV to -4 to2V
Three Axis Magnetometer (TAM) B_x, B_y, B_z	δN_e	70 or 35 Hz	$3 - 10^5$ nT
$\delta N_e - RelativeElectronDensity, \delta N_i - RelativeIonDensity$ $T_e - ElectronTemperature, E - ElectricField, V_p - PlasmaPotential$ $V_f - FloatingPotential, N_e - ElectronDensity$			

5.3 PSPICE Model of Current Collection

We use analog behavioral modeling capabilities of Personal Computer Simulation Program with Integrated Circuit Emphasis (PSPICE) [24] to study the current collection process of a Langmuir probe on a CubeSat. Figure 5.2 represents the PSPICE circuit representation. Figure 5.3 represents the sub-circuit of the collecting surfaces. The SLP with internal heating is modeled as contamination free. However, a spacecraft surface is prone to be non-uniform in conductivity and we add a resistor and capacitor to model dielectric behavior. The nonlinearity current collection from the plasma sheath is modeled as a capacitor in parallel with a voltage (plasma-to-surface) controlled current collection sub-circuit. Since the problem of surface area is the main focus of this study, surface structure variability is not embedded into the circuit.

Table 5.2: Collecting areas.

CubeSat/SLP 10	SLP	CubeSat
Effective Surface(sq. m)	125e-4	125e-4
Cross Sectional Area(sq. m)	2.85e-4	78e-4
Photoemissive Area(sq. m)	2.23e-4	50e-4

The voltage controlled current sources are modeled using the equations for a mesothermal, collisionless and non-magnetized Maxwellian plasma. The current equations also need to account for photocurrent. The spacecraft is modeled as a cylinder and the probes as spherical conductors. The current equations used are described next.

The retardation region currents are

$$I_{\text{ret}} = I_{\text{th}} \exp\left(\frac{q\left(\phi - \phi_p\right)}{K_b T}\right). \tag{5.1}$$

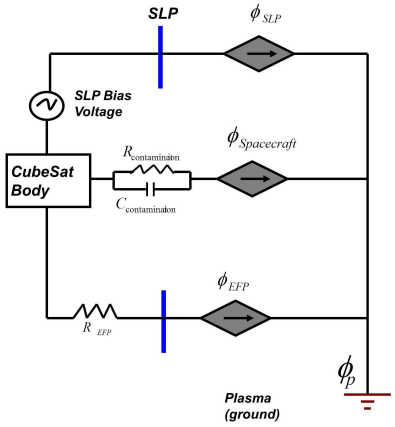

Fig. 5.2: PSPICE circuit representation.

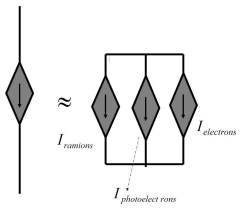

Fig. 5.3: Current collector subcircuit.

The ion saturation currents are

$$I_{\text{sat}} = I_{\text{th}} \frac{2}{\sqrt{\pi}} \left(1 + \frac{q\left(\phi - \phi_p\right)}{K_b T} + \frac{m\nu_{drift}^2}{KbT} \right)^{1/2}. \tag{5.2}$$

The electron saturation region currents for the probes

$$I_{\text{sat}} = I_{\text{th}} \left(1 + \frac{q\left(\phi - \phi_p\right)}{K_b T} \right). \tag{5.3}$$

The electron saturation region of the spacecraft is modeled using the unsimplified version of OML equation [41] due to a discontinuity at the plasma potential (Refer Appendix C for more information).

$$I_{\text{sat}} = I_{\text{th}} \left[\frac{2\sqrt{\eta}}{\sqrt{\pi}} + \exp^{\eta} \left(1 - \left(\sqrt{1 - \exp^{\frac{4\eta}{\pi}}} \right) \right) \right]. \tag{5.4}$$

The symbols and notations used here are already defined in Chapter 2. In equation (5.4) $\eta = \frac{q(\phi - \phi_p)}{K_b T}$. The photoelectric current [42] is modeled as $J_{\text{ph}} A_{\text{ph}} \exp^{\frac{q(\phi - \phi_p)}{V_{ph}}}$, if $\phi - \phi_p > 0$. I_{ph}, A_{ph}, and V_{ph} are the photoelectric current density, photo-emissive area, and the photoionization potential, respectively. When $\phi - \phi_p < 0$, the photoelectric current is a constant which depends on the material.

5.4 Simulation Results of the Langmuir Probe Performance Model

The SLP voltage measurements shown in fig. 5.4 exhibit a nonlinear behavior in the electron saturation regions. They are shifted and warped with respect to the bias voltage. The nonlinearity is observed to be co-related to the spacecraft ground variations. The warping can be seen in the SLP currents in fig. 5.4. The actual voltage applied to the probe is reduced as seen in fig. 5.5, and hence the current collected would be reduced. But not accounting for this reduction, would lead to an over-estimation of effective probe-plasma-potential and the effect of which is seen in next section.

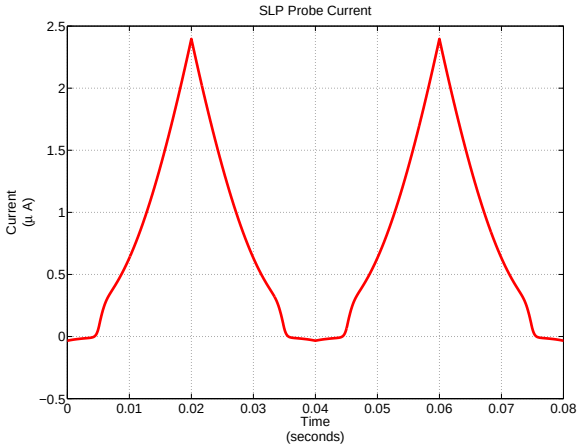

Fig. 5.4: SLP probe current simulation.

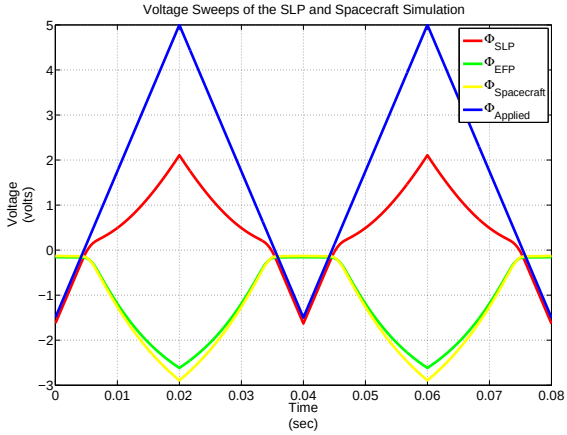

Fig. 5.5: Voltage sweeps of the SLP and spacecraft simulation.

5.5 Simulation Results to Illustrate the Surface Area Ratio Effect on the Determination of Plasma Parameters

We plot the I-V curves that would be generated for the warped voltage and the applied bias voltage and do a reverse-engineering of deducing the plasma parameters in this section.

Apparent SLP voltage curve in fig. 5.6 refers to the I-V curve generated when the bias voltage on the probe is used. The actual current collected is due to a reduced potential, shown in fig. 5.5. Hence when plotted as the bias voltage characteristic, the curve gets stretched and shifted due to charging of the spacecraft surface. To gauge the effect of the

warped I-V characteristic, we do a least-square-fit analysis for the synthetic data from the model and determine the corresponding plasma properties. We can see from fig. 5.7 that the temperature is over-estimated and the density measurement is affected, too.

5.6 How Do We Correct the Measurements?

It was seen from the STORMS data analysis that using the floating potential to gauge the spacecraft reference potential is an accurate technique of accounting for the Surface Area Ratio effects.

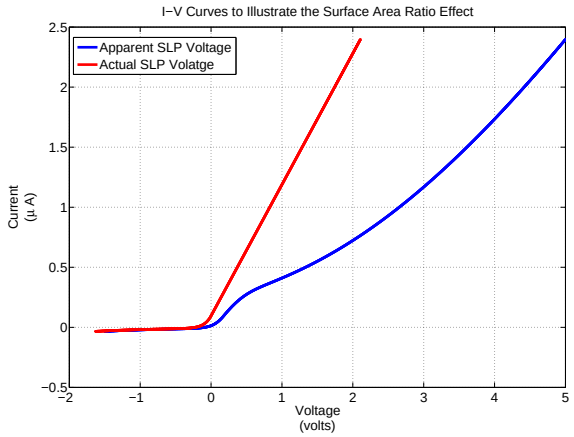

Fig. 5.6: I-V curves of the slp for the bias voltage and the warped voltage.

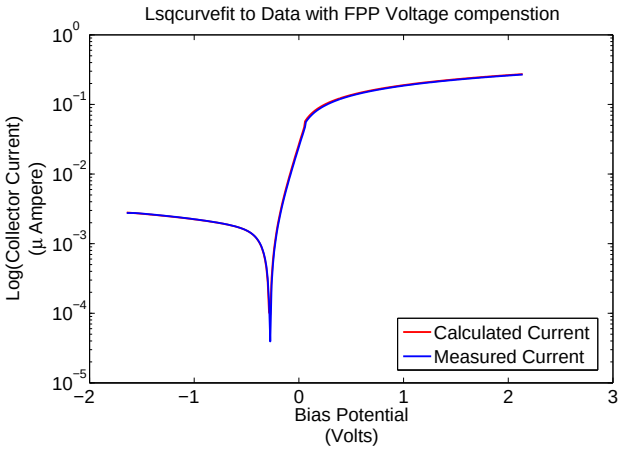

Fig. 5.7: Lsqcurvefit to synthetic data generated from the simulation to measure plasma properties using the apparent slp voltage curves.

It can be seen from fig. 5.5 that the EFP measures the spacecraft charging. EFP which is an electrically isolated probe floats to the spacecraft charging potential with respect to the plasma. We can thereby use this value to calculate the actual voltage present between the SLP surface and the plasma, as seen from fig. 5.5. Now we repeat the curve fit to the synthetic data but with Surface Area Ratio effects considered. Therefore, we can calculate the SLP voltage by $\phi_{SLP} = \phi_{BiasVoltage} + \phi_{EFP}$.

We can see that SLP measurements are corrupted by the charging effects of the CubeSat. The temperature and the density measurements are wrongly estimated. Though the curvefits for both the cases agree with the theory, the values determined from the least square fitting is erroneous for the apparent voltage case (fig. 5.8). However, EFP measurements could be used to determine the actual potential from the SLP surface to the plasma. We can see that this would give a good representation of the slope, hence giving right temperature values. By using this technique, we can make accurate measurements. Thereby, we conclude that we can make reliable SLP measurements, only if we have an EFP on the CubeSat.

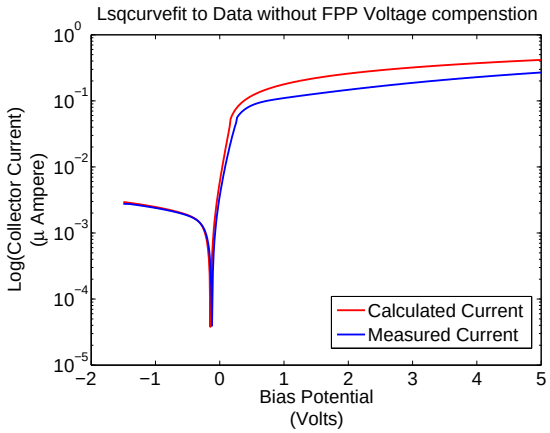

Fig. 5.8: Illustration of surface area ratio effects.

Chapter 6

Conclusion

Langmuir probes have been popularly flown on numerous space missions as plasma diagnostic instruments. Though simple in design, their effectiveness in making accurate measurements is contingent upon the accurate application of current collection theories/models. These theories model the interwoven constraints of the probe electronics and surrounding plasma sheath on the current collection process. The surface morphology (size and structure) of the probe is one such factor which needs to be correctly established for accurate plasma analysis.

Surface structure defined in terms of work function, influences the probe-plasma potential. Numerous factors such as contamination bring out spatial and temporal variation of the surface structure during the flight of the probe. These variations cannot be completely ruled out using design measures alone. We developed a mathematical framework for defining the probe behavior in the event of surface non-uniformity in Chapter 2. A sounding rocket mission with a Langmuir probe which was subjected to a structurally disturbed surface behavior was analyzed using the work-function-variation model derived in this paper. The significance of using a comprehensive model which accounts for the plasma behavior and the probe behavior was shown in Chapter 4. The importance of defining the plasma and probe behavior thoroughly was illustrated in Chapter 4. It was seen that absence to account for the surface variations would lead to surface size dependency, which is a major factor on small satellite based missions were inspected in Chapter 5. It was seen that the Langmuir probe exhibits a warped current collection and that only way one can make accurate measurements is to fly floating potential probes in tandem with the sweeping Langmuir probes. The study was done for an upcoming USU/SDL small satellite effort named DICE.

The probe theory developed in this paper could be expanded in various directions. One

of which would be to embed the wake-area collection dynamics into the equations. It has been observed in earlier regression analysis studies as well as in this paper that the geometry factor exhibits a marked variation from the fixed value of 0.5. A way of expressing the wake dependency into the equations instead of fitting would fine tune the plasma analysis further. Currently particle-in-cell simulations are the only form of study used for wake-region current dynamics. These require tremendous computational powers and developing a theory which would embed wake region effects would be an ideal and elegant way of plasma analysis. We can also add magnetic field and collision effects in to the model thus extending into regimes beyond the Earth's ionosphere.

The probe theory developed does not accounting for contaminants like water which are completely prevented by design measures. Developing a theory which incorporates the effect of non-reactive contaminants would ensure the availability of a completely theoretical approach of handling the problem of surface structure non-uniformity.

Another approach would be to develop a new technique of analyzing the data. Bayesian techniques like Kalman filters would be an interesting approach for looking into the probe current data sets. The surface area ratio effects were investigated on the current collection dynamics alone. The PSPICE model developed could be further zoomed-in at the transistor levels to study the probe behavior under various plasma conditions.

Thus, it would be fitting to conclude that though a comprehensive probe theory and data-analysis algorithm was derived in this paper, there are various directions in which this work could be further progressed. The small satellite missions run on cost constraints would not be able to employ elaborate design measures to account for all possible variations in current collection dynamics. Hence, developing a probe theory or model which mathematically provides a framework to account for these variations would be highly lucrative and useful for space plasma analysis.

References

[1] J. D. Swift and M. J. R. Schwar, *Electric Probes for Plasma Diagnostics*. London: Iliffe, 1970.

[2] L. H. Brace, "Langmuir probe measurements in the ionosphere," *Measurement Techniques in Space Plasmas: Particles*, pp. 23–35, 1998.

[3] H. M. Mott-Smith and I. Langmuir, "The theory of collectors in gaseous discharges," *Physical Reviews*, vol. 28, pp. 727–763, 1926.

[4] J. R. Sanmartin, "Theory of a probe in a strong magnetic field," *Physics of Fluids*, vol. 13, pp. 103–116, 1970.

[5] W. R. Hoegy and L. E. Wharton, "Current to a moving cylindrical electrostatic probe," *Journal of Applied Physics*, vol. 44, no. 12, pp. 5365–5371, 1973.

[6] G. Medicus, " Spherical Langmuir Probe in "Drifting" and "Accelerated" Maxwellian Distribution," *Journal of Applied Physics*, vol. 33, no. 10, pp. 3094–3100, 1962.

[7] J. Rubinstein and J. G. Laframboise, "Theory of a spherical probe in a collisionless magnetoplasma," *Physics of Fluids*, vol. 25, no. 7, pp. 1174–1182, 1982.

[8] A. Barjatya and C. M. Swenson, "Observations of triboelectric charging effects on Langmuir-type probes in dusty plasma," *Journal of Geophysical Research*, no. A10302, 2006.

[9] H. B. Michaelson, "The Work function of the elements and its periodicity," *Journal of Applied Physics*, vol. 48, no. 11, pp. 4729–4733, 1977.

[10] P. Hoffmann, "Work function: Lecture notes on surface science," [http://philiphofmann.net/surflec3/index.html].

[11] R. L. Park and M. G. Lagally, *Methods of Experimental Physics-Volume 22, Solid State Physics-Surfaces*. London: Academic Press, 2004.

[12] J. B. Camp, T. W. Darling, and R. E. Brown, "Macroscopic variations of surface potentials of conductors," *Journal of Applied Physics*, vol. 69, no. 10, pp. 7126–7129, May 1991.

[13] M. Wahlstrom, E. Johansson, E. Veszelei, P. Bennich, M.Olsson, and S. Hogmark, "Improved Langmuir probe surface coatings for the Cassini satellite," *Thin Solid Films*, vol. 220, no. 1-2, pp. 315–320, Nov. 1992.

[14] M. Veszelei and E. Veszelei, "Optical properties and Equilibrium Temperatures of Titanium-Nitride and Graphite-Coated Langmuir Probe for Space Applications," *Thin Solid Films*, vol. 236, no. 1-2, pp. 46–50, Dec. 1993.

[15] K. Hirao and K. Oyama, "Inaccuracies in electron density estimates due to surface contamination of langmuir probes," *Planetry and Space Science*, vol. 24, no. 1, pp. 87–89, Jan. 1976.

[16] W. E. Amatucci, M. E. Koepke, T. E. Sheridan, M. J. Alport, and J. J. Carroll, "Self cleaning Langmuir probe," *Review of Scientific Instruments*, vol. 64, no. 5, pp. 1253–1256, May 1993.

[17] W. E. Amatucci, P. W. Schuck, D. N. Walker, P. M. Kintner, S. Powell, B. Holbeck, and D. Leonhardt, "Contamination free sounding rocket Langmuir probe," *Review of Scientific Instruments*, vol. 72, no. 4, pp. 2052–2057, 2001.

[18] T. L. Thomas and E. L. Battle, "Effects of Contamination on Langmuir Probe Measurements in Glow Discharge Plasmas," *Journal of Applied Physics*, vol. 41, no. 8, pp. 3428 – 3432, Jul. 1970.

[19] M. Hirt, C. T. Steigies, and A. Piel, "Plasma diagnostics with Langmuir probes in the equatorial ionosphere: II. Evaluation of DEOS flight F06," *Journal of Physics D: Applied Physics*, vol. 34, p. 26502657, 2001.

[20] C. T. Steigies, R. F. Pfaff, and D. E. Rowland, "Surface Property effects on Langmuir Probes launched on sounding rockets," Proceedings of the 17th ESA Symposium on European Rocket and Balloon Programmes and Related Research. ESA SP-590, 2005.

[21] K. I. Oyama, "A systematic investigation of several phenomena associated with contaminated Langmuir probes," *Planetary and Space Science*, vol. 24, no. 2, pp. 183–190, Feb. 1976.

[22] A. Piel, M. Hirt, and C. Steigies, "Plasma diagnostics with Langmuir probes in the equatorial ionosphere: I. The influence of surface contamination," *Journal of Physics D: Applied Physics*, vol. 34, pp. 2643–2649, 2001.

[23] E. P. Szuszczewicz, "Area influences and floating potentials in Langmuir probe measurements," *Journal of Applied Physics*, vol. 43, no. 3, pp. 874–880, Mar. 1972.

[24] A. Barjatya, *Langmuir Probe Measurements in the Ionosphere*. Ph.D. dissertation, Utah State University, Logan, UT, 2007.

[25] M. Kelley, *The Earths Ionosphere: Electrodynamics and Plasma Physics*. San Diego: Academic Press, 1989.

[26] R. W. Schunk and A. F. Nagy, *Ionospheres- Physics, Plasma Physics, and Chemistry*, ser. Atmospheric and Space Science Series. Cambridge: Cambridge University Press, 2000.

[27] "Introduction to hf radio propagation," [http://www.ips.gov.au].

[28] P. Bhaneja, G. D. Earle, R. L. Bishop, T. W. Bullett, J. Mabie, and R. Redmon, "A statistical study of midlatitude spread F at Wallops Island," *Journal of Geophysical Research*, vol. 114, no. A04301, 2009.

[29] G. D. Earle, P. Bhaneja, P. A. Roddy, C. M. Swenosn, A. Barjatya, R. L. Bishop, T. W. Bullett, G. Crowley, R. Redmon, K. Groves, R. Cosgrove, and S. L. Vadas, "A Comprehensive Rocket and Radar Study of Midlatitude Spread F," *Journal of Geophysical Research*, vol. 115, 2010.

[30] I. Katz, G. Jongeward, V. Davis, T. Morton, and D. Ferguson, "Current collection by a large Langmuir probe in a mesothermal (ram) plasma," *Measurement Techniques in Space Plasmas: Particles*, vol. 102, no. 3, pp. 37–41, 1998.

[31] J. Gregory, "Design, test and calibration of the utah state university floating potential probe," Master's thesis, Utah State University, Logan, UT, 2009.

[32] A.Hummel, "The plasma impedance probe: A quadrature sampling," Master's thesis, Utah State University, Logan, UT, 2006.

[33] H. G. James, "RF Charging of Topside Sounder Spacecraft," *6th Spacecraft Charging Technology Conference, AFRL-VS-TR-20001578*, vol. 35, Sep. 2000.

[34] H. G. James, "Discharge of RF-Induced Spacecraft DC Potential by Postive Ions," *Planetary and Space Science*, vol. 35, pp. 105–108, 1987.

[35] C. Swenson, *Spacecraft Instrumentation: Langmuir Probes, ECE 7210 Notes, Utah State University.* Logan, UT: Electrical and Computer Engineering, Utah State University, 1989.

[36] A. Barjatya, C. M. Swenson, D. C. Thompson, and K. W. Jr, "Data analysis of the floating potential measurement unit aboard the international space station," *Review of Scientific Instruments*, vol. 80, no. 4, Apr. 2009.

[37] S.Patra, "Electron density and electron neutral collision frequency in the ionosphere using plasma impedance probe measurements on sounding rockets," Master's thesis, Utah State University, Logan, UT, 2009.

[38] E. Spencer, S. Patra, T. Andriyas, C. Swenson, J. Ward, and A. Barjatya, "Electron density and electron neutral collision frequency in the ionosphere using plasma impedance probe measurements," *Journal of Geophysical Research*, vol. 113, no. A09305, 2008.

[39] G. Crowley, C. S. Fish, G. S. Bust, C. M. Swenson, A. Barjatya, and M. F. Larsen, "Dynamic ionosphere cubesat experiment (dice)," *EOS Trans. AGU, Abstract SM42A-06(90(52)):Fall Meet. Suppl*, Dec. 2009.

[40] E. M. Stromberg, S. Burr, D. Hui, and C. M. Swenson, "Electric field wire boom system and instrument for cubesats," *EOS Trans. AGU, Abstract SM33C-1578(90(52)):Fall Meet. Suppl., 2009*, Dec. 2009.

[41] J. E. Allen, "Probe Theory- The Orbital Motion Approach," *Physica Scripta*, vol. 45, pp. 497–503, 1992.

[42] R. J. L. Grard, "Properties of the satellite photoelectron sheath derived from photoemission laboratory measurements," *Journal of Geophysical Research*, vol. 78, no. 16, pp. 2885–2906, 1973.

Appendices

Appendix A

PCM Telemetry Matrix

The telemetry matrix is depicted in fig. A.1. The overall telemetry bit rate is 2.5 MHz resulting is a major frame rate of about 76.3 Hz. Columns 4-8 and 20-25 are the data channels of the Impedance probe implementations, namely, the SIP and PFP. The SIP is sampled twice every minor frame and results in real and imaginary absolute impedance measurements, real and imaginary impedance minus the free space capacitance measurements, and absolute impedance magnitude measurements. Also, the free space capacitance is recorded once every major frame. Multiplexing the PFP results in a 32-bit word that is divided into the low-order and high-order bits and sampled once every two minor frames. Columns 2-3, 10-11, 18-19, and 26-27 are the SLP data channels labeled LG and HG. The SLP performs one 1024-point sweep which takes 52.4 milliseconds. These sweeps are made every twenty seconds and otherwise held at a constant 3 Volts. This data is captured in four high-gain and four low-gain samples that are symmetrically sampled in each minor frame. The DCP data is transmitted once every minor frame with the low gain and high gain channel measurements made every alternative minor frame.

The FPP channels are depicted in columns 12-16 labeled VS1, VS2, VS3, VS4, and Vlsb. Data from all of the four FPP probes is simultaneously transmitted as four 16-bit samples every minor frame. The Vlsb channel data was found to be highly noisy, and hence was not used in the calibration process. The data from the PCM matrix is extracted and converted from counts to the respective measurements units using the calibration constants.

	1	2	3	4	5	6	7	8	9	10	11	12	13	14	15	16
1	SFID	LG	HG	SIPR	SIPRD	SIPI	SIPID	SIPM	DCPH	LG	HG	V1S	V2S	V3S	V4S	Vlsb
2									DCPL							
3																
4																
5																
6																
57																
58																
59																
60																
61																
62																
63	↓	↓	↓	↓	↓	↓	↓	↓	DCPH	↓	↓	↓	↓	↓	↓	↓
64	SFID	LG	HG	SIPR	SIPRD	SIPI	SIPID	SIPM	DCPL	LG	HG	V1S	V2S	V3S	V4S	Vlsb

	17	18	19	20	21	22	23	24	25	26	27	28	29	30	31	32
1	GPS	LG	HG	SIPR	SIPRD	SIPI	SIPID	SIPM	PFPL	LG	HG	A1	A3	T1A	SYNC	SYNC
2									PFPH			PIP	A0	T1B		
3												A2	A4	Spare		
4												SLP	A5			
5												A1	A3			
6												PIP	A6			
58												PIP	A25			
59												A2	A26			
60												SLP	A28			
61												A1	A3			
62												PIP	A29			
63	↓	↓	↓	↓	↓	↓	↓	↓	PFPL	↓	↓	A2	A30	↓	↓	↓
64	GPS	LG	HG	SIPR	SIPRD	SIPI	SIPID	SIPM	PFPH	LG	HG	Co	A31	Spare	SYNC	SYNC

Fig. A.1: Telemetry matrix.

Appendix B

STORMS Data Survey Plots for SLP Sweeps

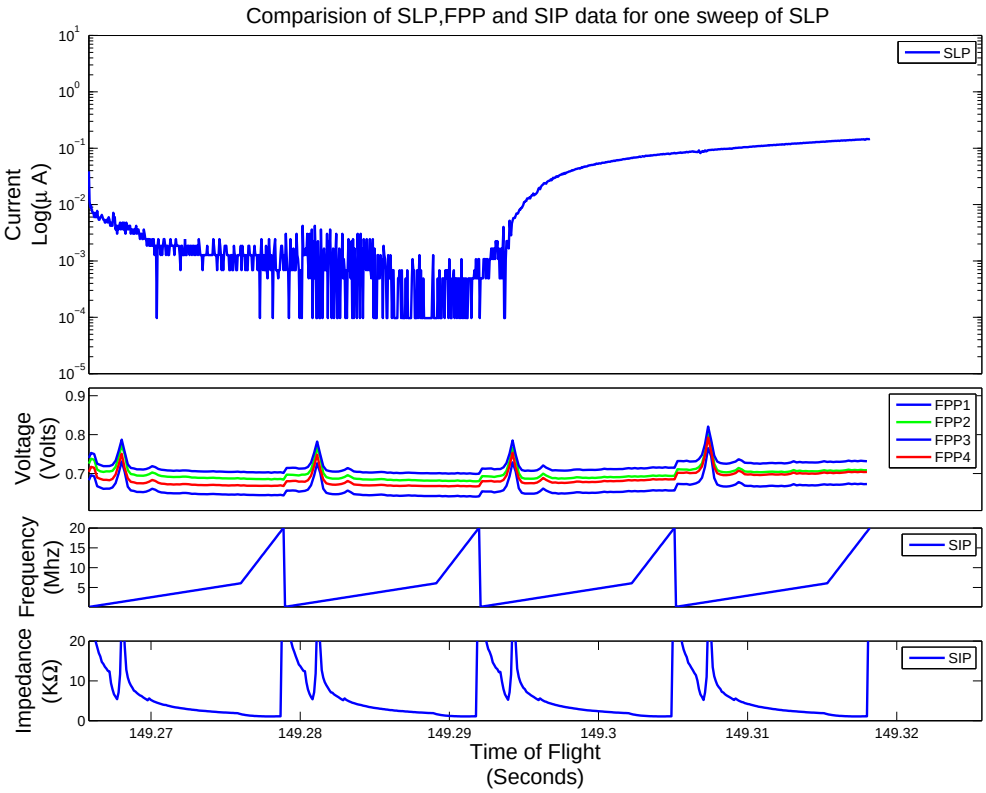

Fig. B.1: Sweep 1: Altitude of 258.62Km.

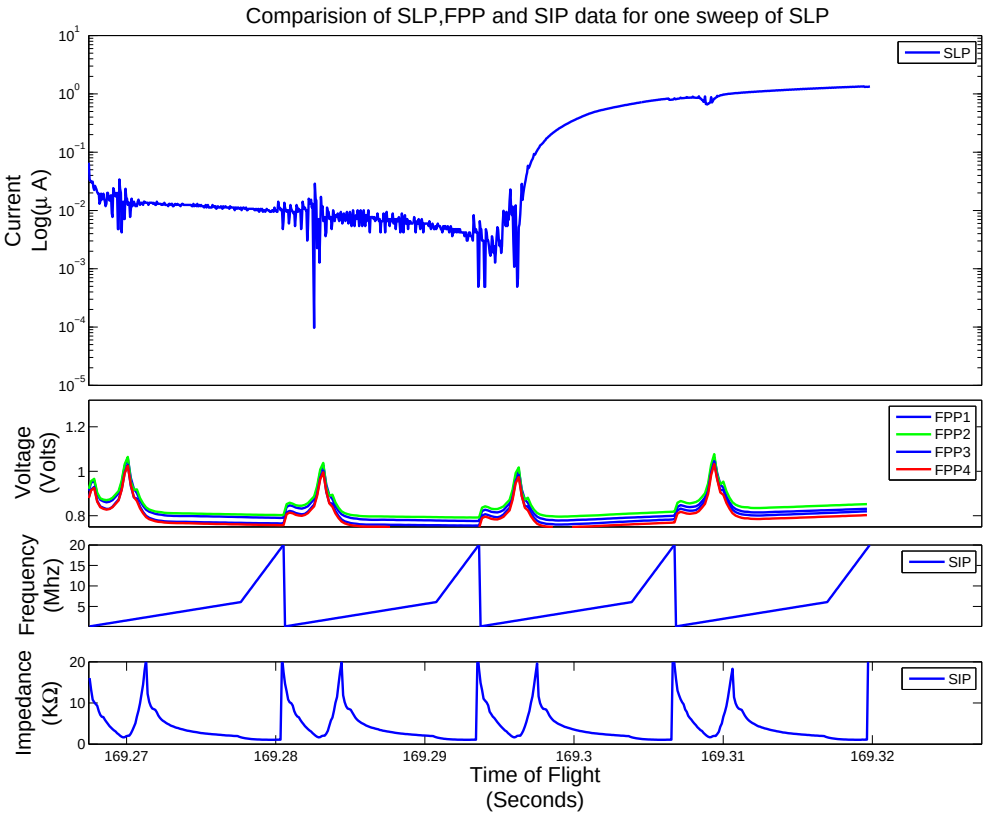

Fig. B.2: Sweep 2: Altitude of 289.18Km.

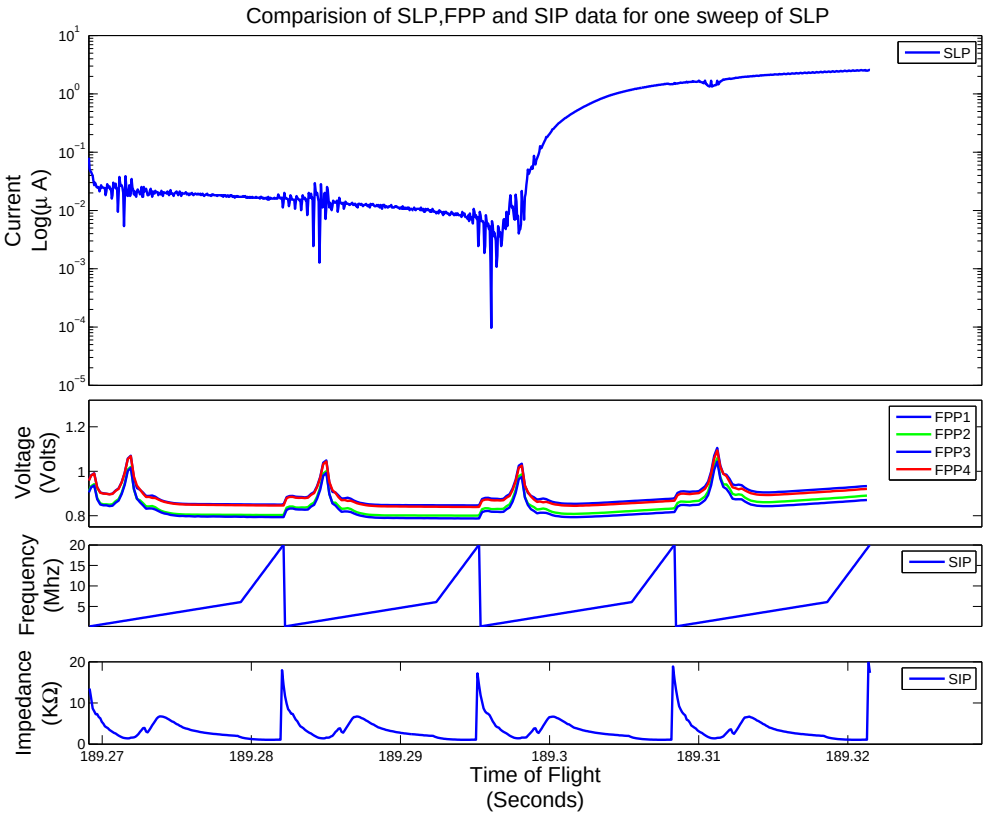

Fig. B.3: Sweep 3: Altitude of 315.59Km.

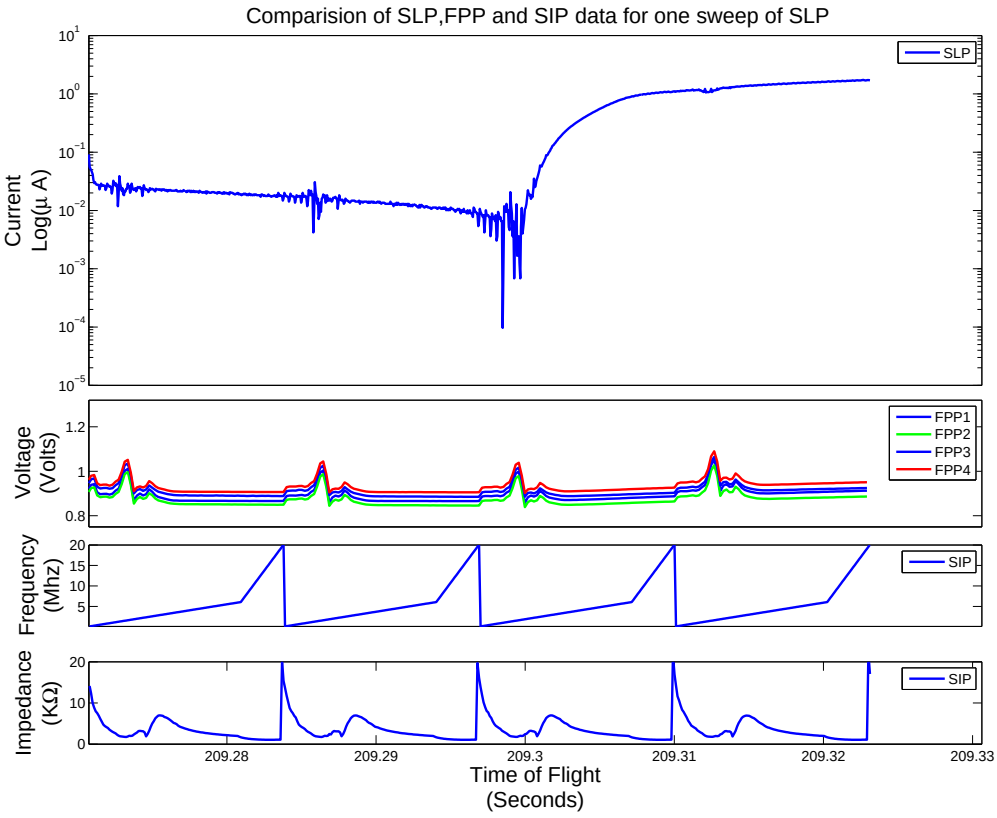

Fig. B.4: Sweep 4: Altitude of 337.82Km.

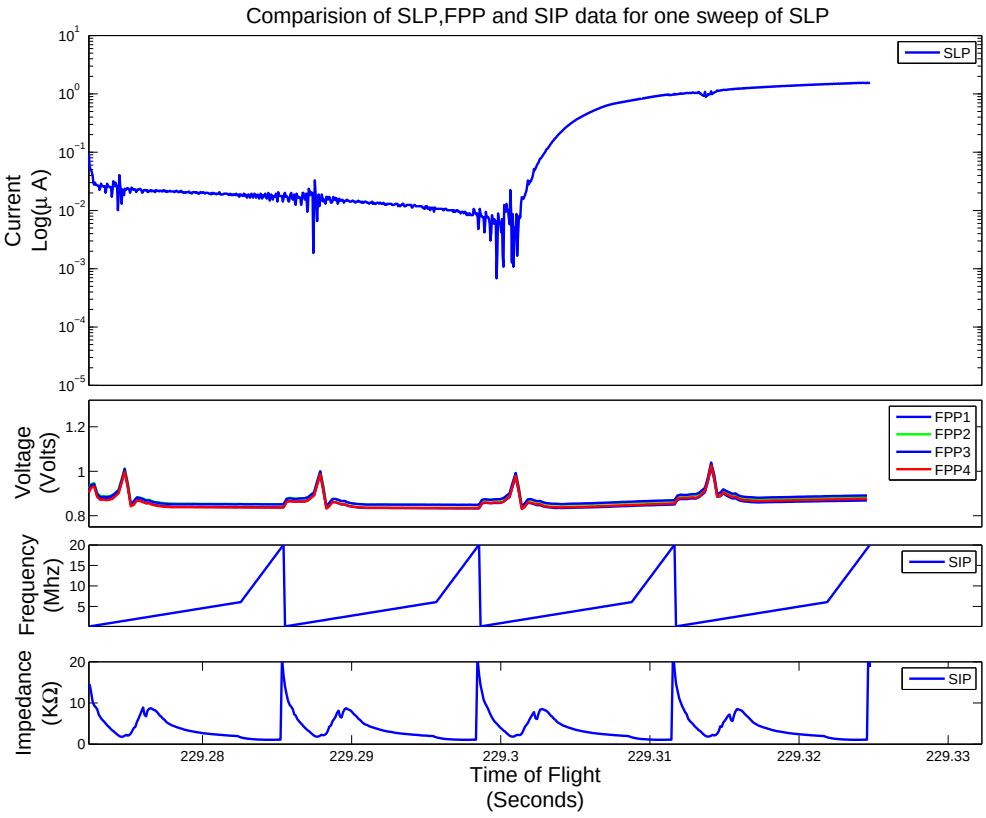

Fig. B.5: Sweep 5: Altitude of 355.97Km.

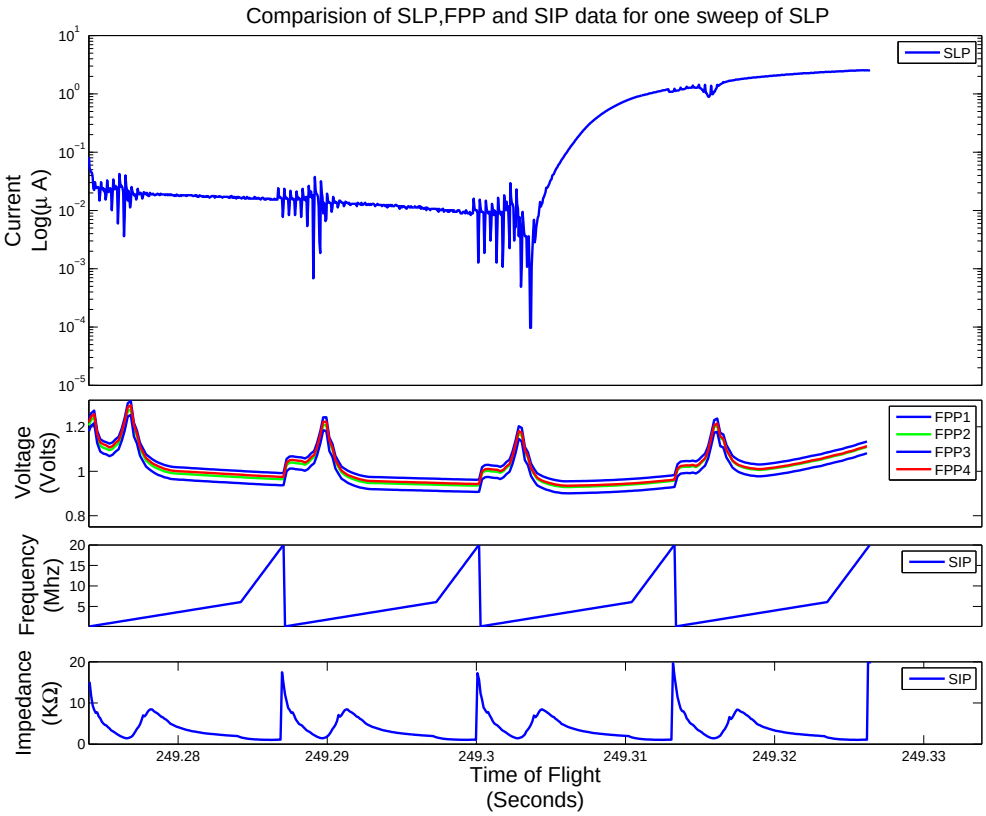

Fig. B.6: Sweep 6: Altitude of 370.21Km.

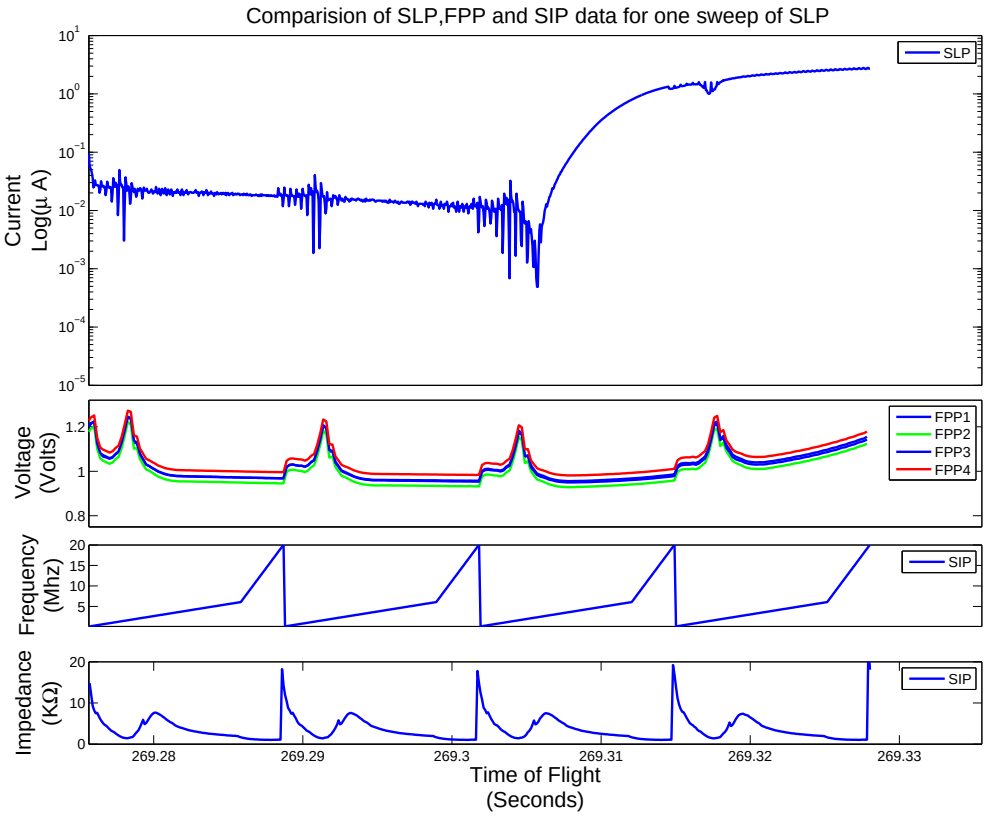

Fig. B.7: Sweep 7: Altitude of 380.79Km.

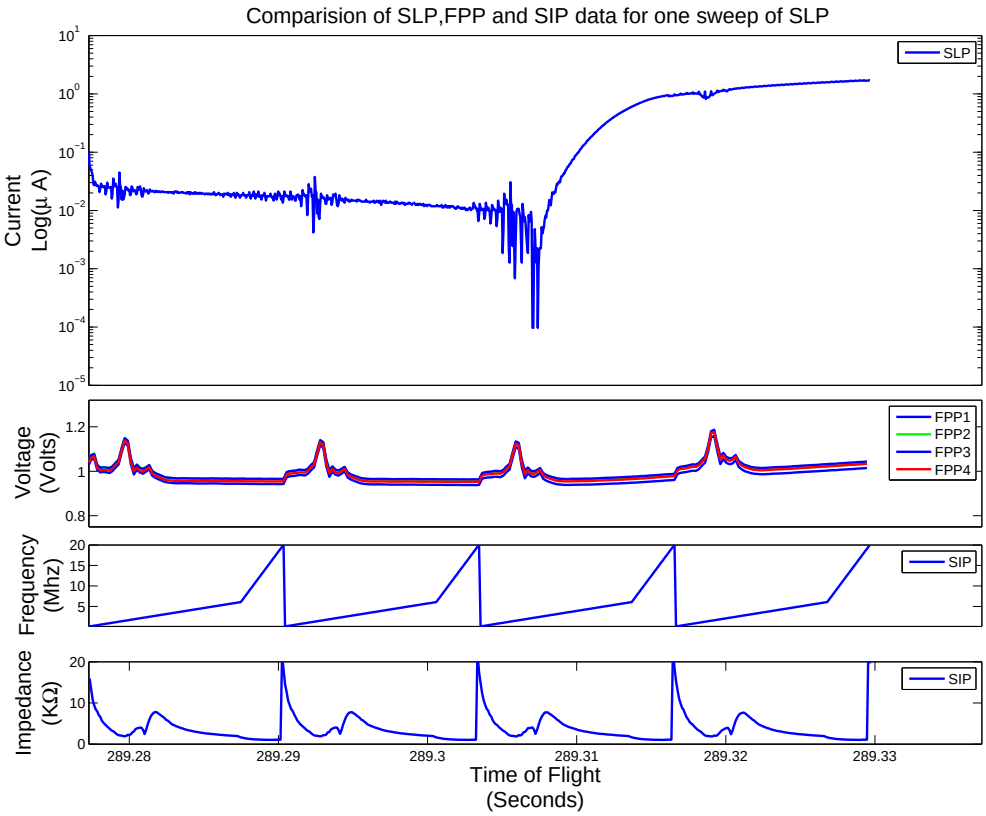

Fig. B.8: Sweep 8: Altitude of 387.92Km.

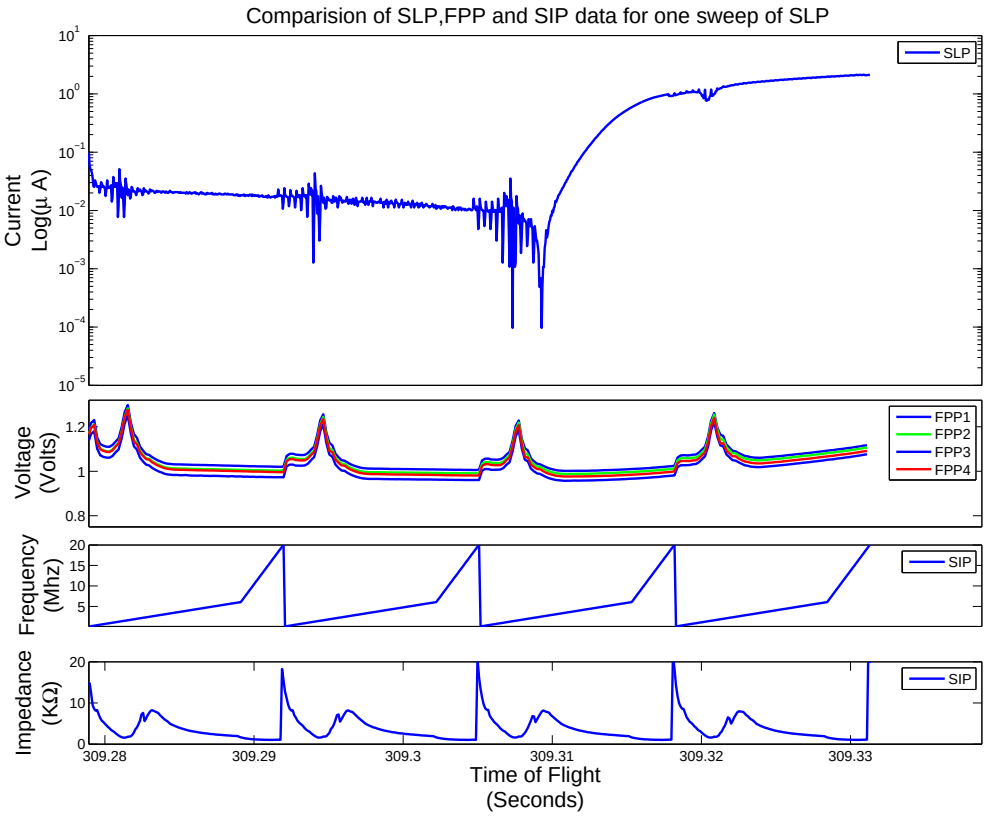

Fig. B.9: Sweep 9: Altitude of 391.79Km.

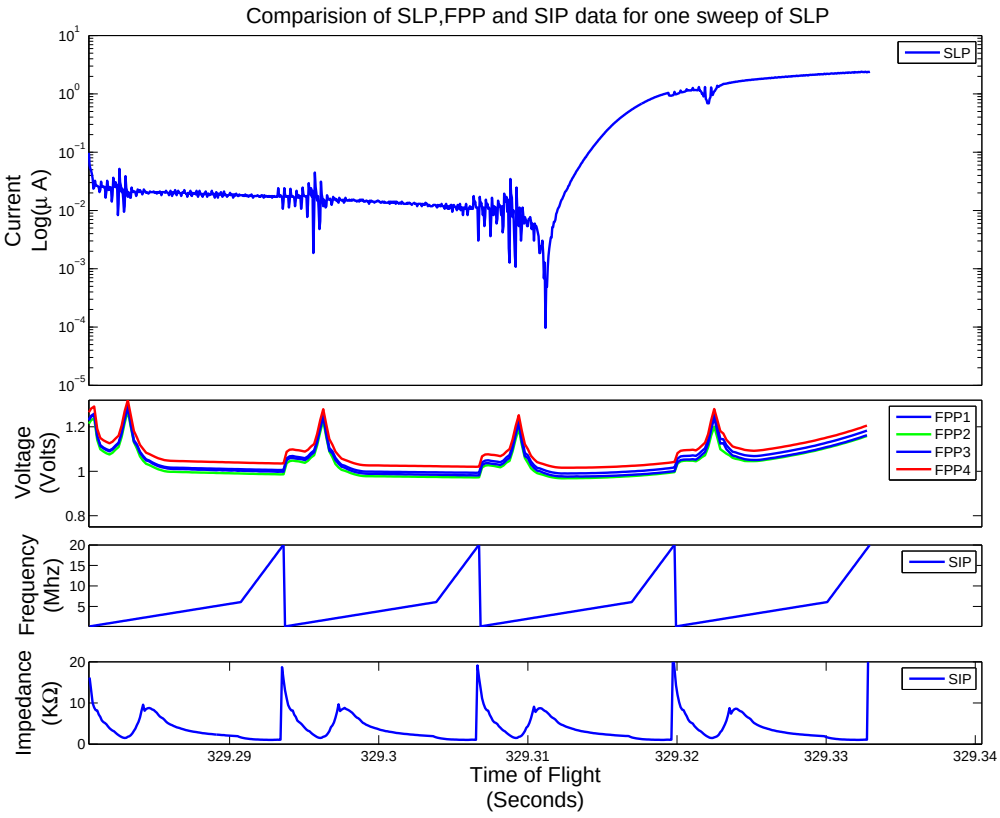

Fig. B.10: Sweep 10: Altitude of 392.53Km.

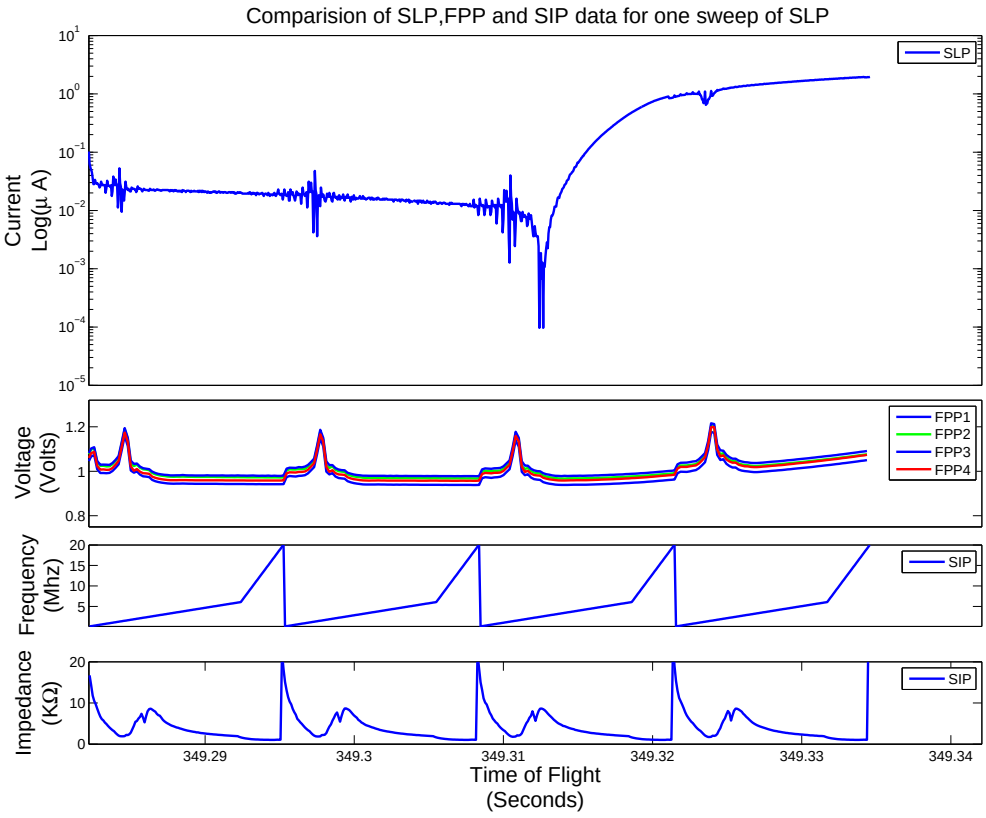

Fig. B.11: Sweep 11: Altitude of 390.20Km.

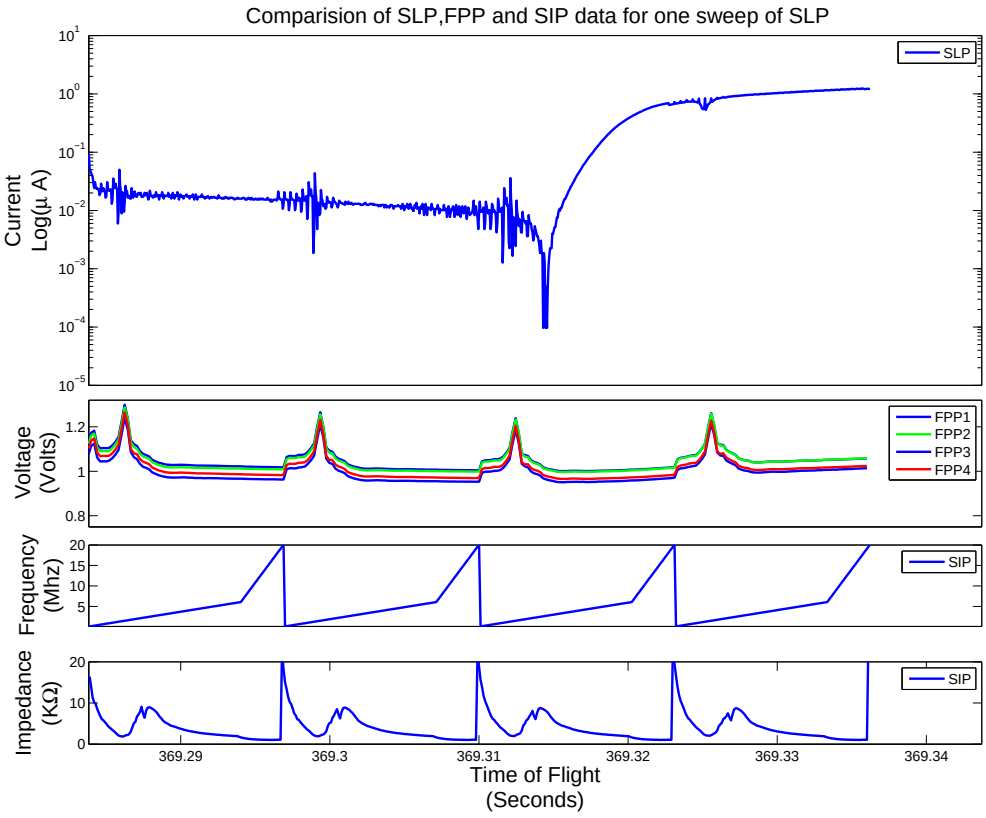

Fig. B.12: Sweep 12: Altitude of 384.78Km.

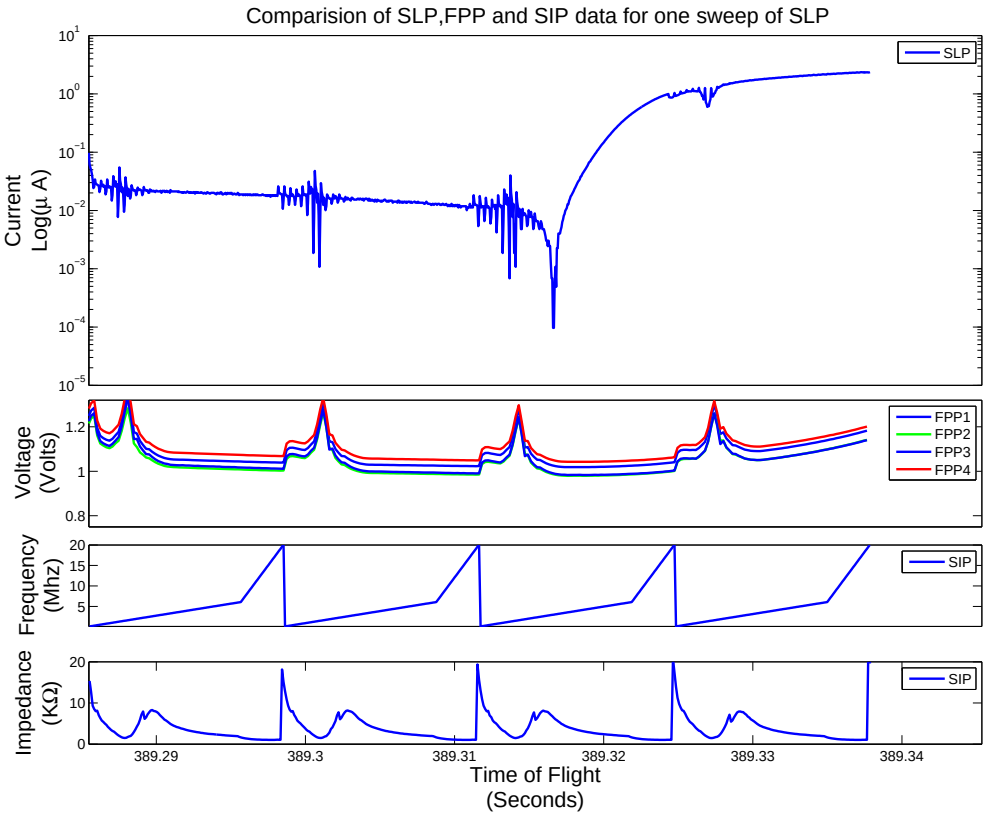

Fig. B.13: Sweep 13: Altitude of 376.18Km.

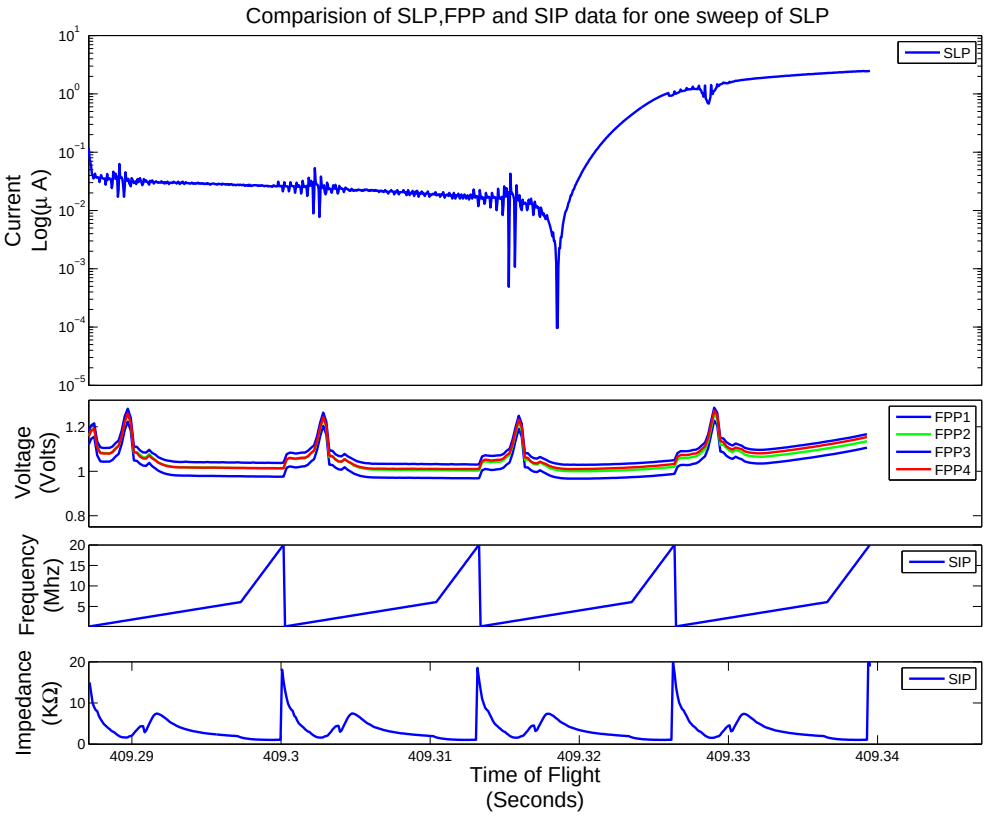

Fig. B.14: Sweep 14: Altitude of 364.26Km.

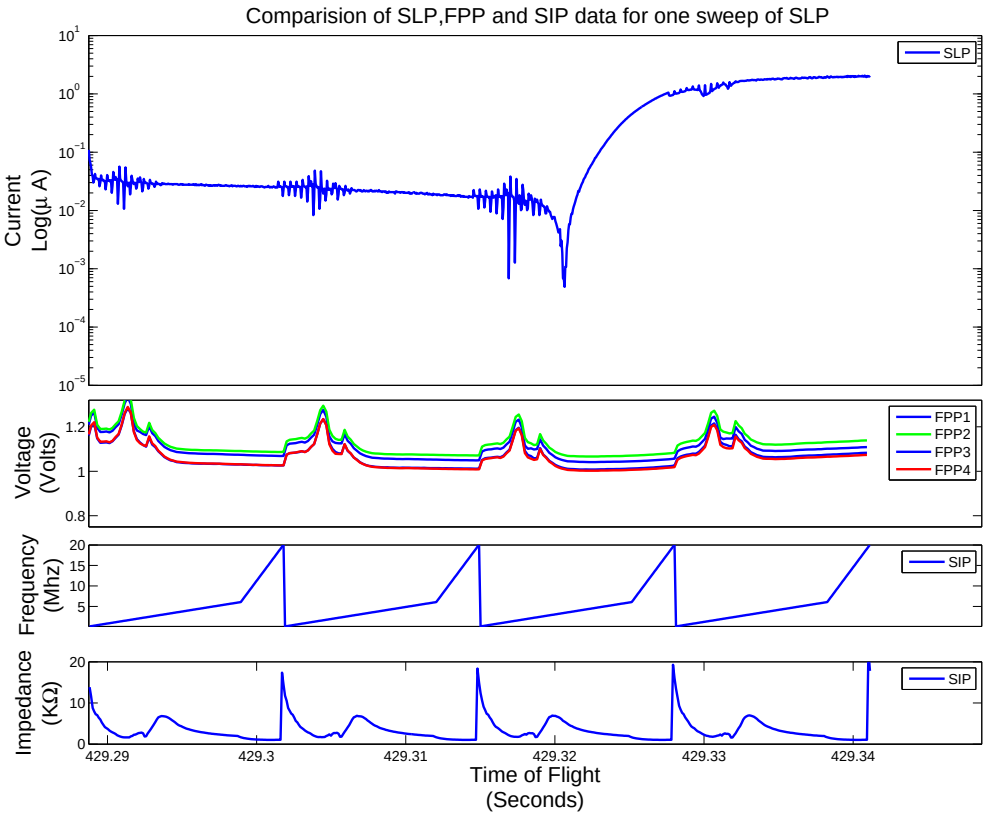

Fig. B.15: Sweep 15: Altitude of 348.81Km.

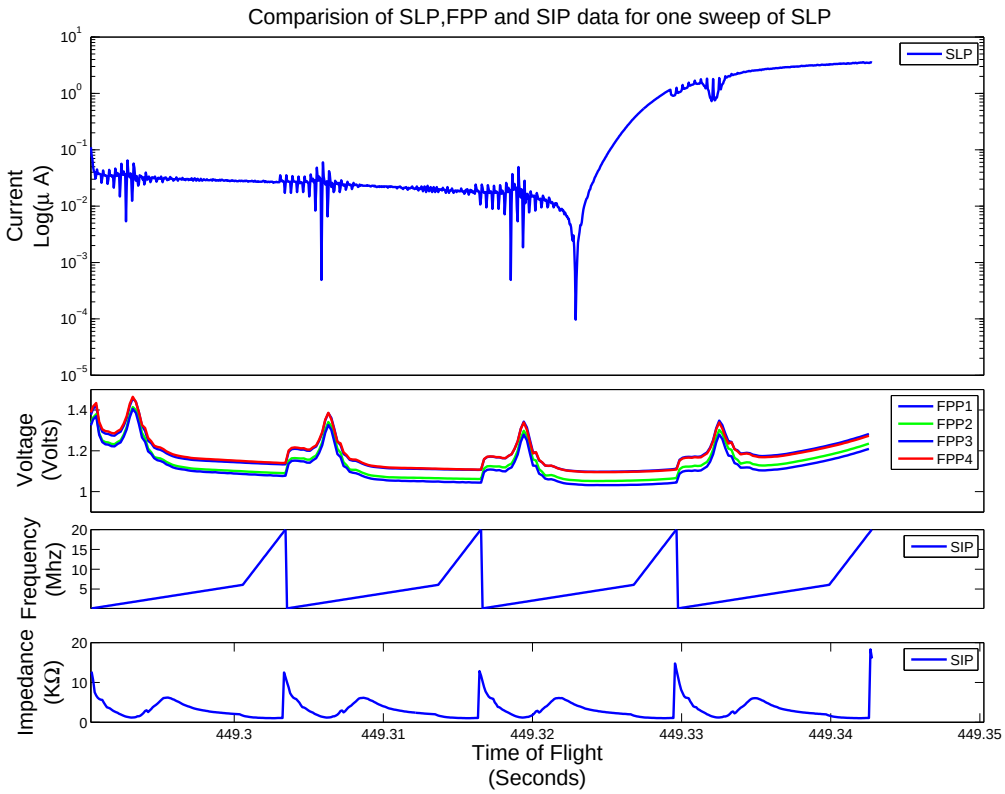

Fig. B.16: Sweep 16: Altitude of 329.62Km.

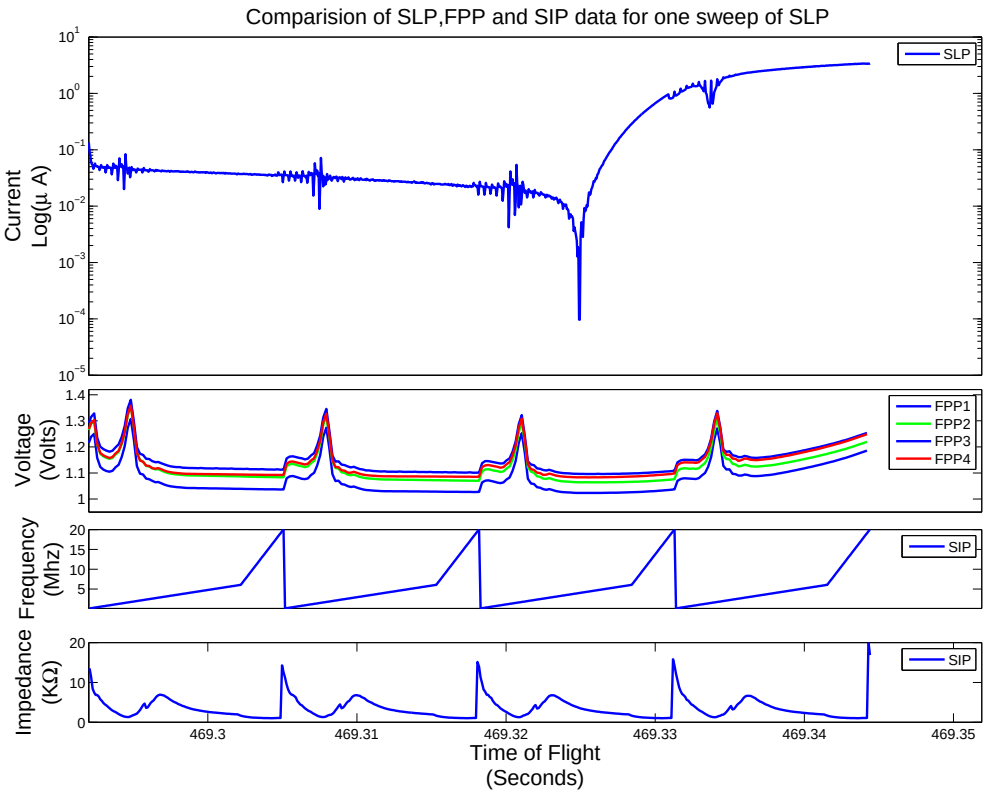

Fig. B.17: Sweep 17: Altitude of 306.52Km.

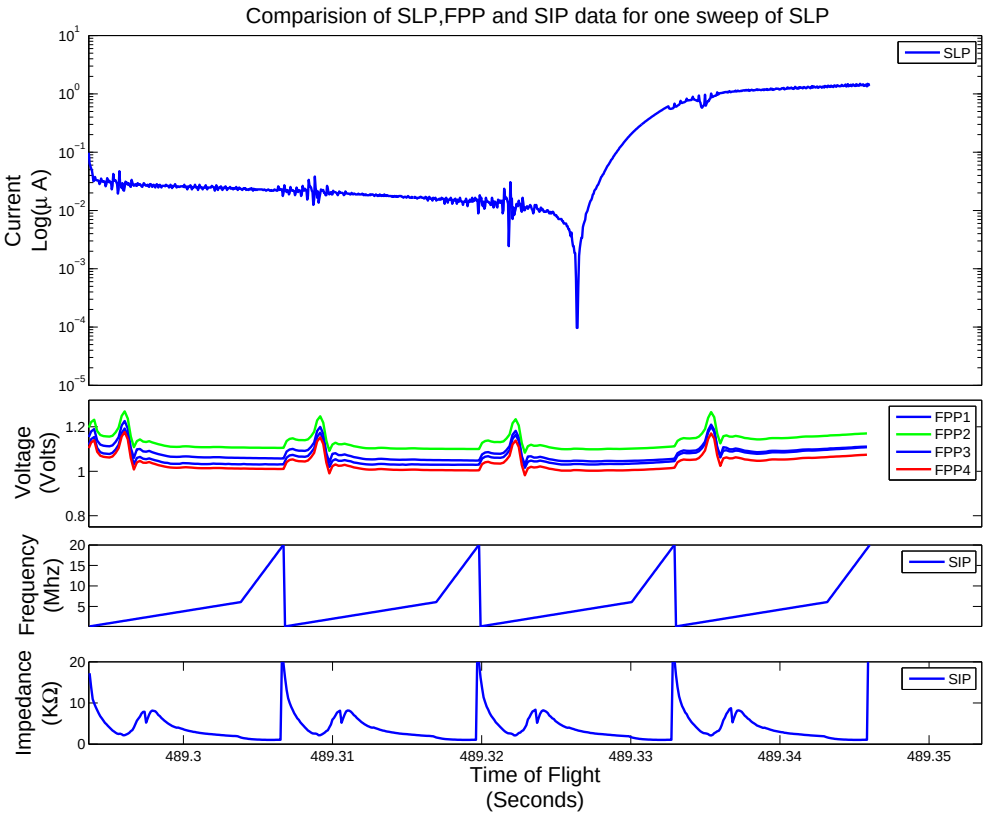

Fig. B.18: Sweep 18: Altitude of 279.38Km.

Appendix C

Cylindrical Probe Electron Current Collection: Dicontinuity at Plasma Potential in OML Theory

The equation for a cylindrical collector given by the OML Theory [3] is

$$I_{\text{sat}} = I_{\text{th}} \frac{2}{\sqrt{\pi}} \left(1 + \frac{q\left(\phi - \phi_p\right)}{K_b T}\right)^{1/2}. \tag{C.1}$$

This is valid for $\frac{q(\phi-\phi_p)}{K_b T} > 2$. For $\frac{q(\phi-\phi_p)}{K_b T} < 2$, the electron current collection is subjected to a discontinuity at the plasma potential. This has been explained in the paper by J. E. Allen [41]. Figure 2 in the paper by Allen [41] has the diagramatic representation of this. The current collection described by (C.1) is obtained by simplifying the original expression

$$I_{\text{sat}} = I_{\text{th}} \left[\frac{2\sqrt{\eta}}{\sqrt{\pi}} + \exp^{\eta}\left(1 - \left(\sqrt{1 - \exp^{\frac{4\eta}{\pi}}}\right)\right)\right]. \tag{C.2}$$

This discontinuity in the equation describing the electron current collection process is due to the fact that the current collection at the voltage step just prior to the plasma potential is almost equal to the electron thermal current. However at plasma potential, the current using (C.1) would be $2/\sqrt{\pi}$ times the electron current if (C.2). This sudden increase in the current at the transition from retardation region to saturation region leads to a discontinuous region around the plasma potential as illustrated by fig. C.1

The equation (C.2) is simplified using the assumption that erf(x) = $2\text{x}/\sqrt{\pi}$ for small x. It can be seen that when equation (C.2) is used, the current at plasma potential is equal to electron thermal current. Hence, for the modeling of the cylindrical spacecraft in Chapter 5 for surface area ratio problem, we have used the expression from Allen's paper, which is the non-simplified version of the OML theory equations in the form of error functions.

However, we do not need to worry about the discontinuity in the formulation of the

surface structure model (work-function-variation model). This is because of the smoothening effect seen around the plasma potential (Chapter 1) which flattens out the discontinuity. The averaging effect explained in Chapter 1 leads to an even transition, and hence we can use the simplified form of OML theory equations. We illustrate our argument by plotting the I-V curves around the plasma potential for probe currents with work function variation model. We have shown the results for std. deviation=0.1 which corresponds to a work function variation of 0.1 volts which is the most probable value of measure of non-uniformity.

We can see from fig. C.2 that for a non-uniform surface, the averaging effect would cause the discontinuity to smoothen out, and hence both non-simplified and simplified OML theory equations are coincident.

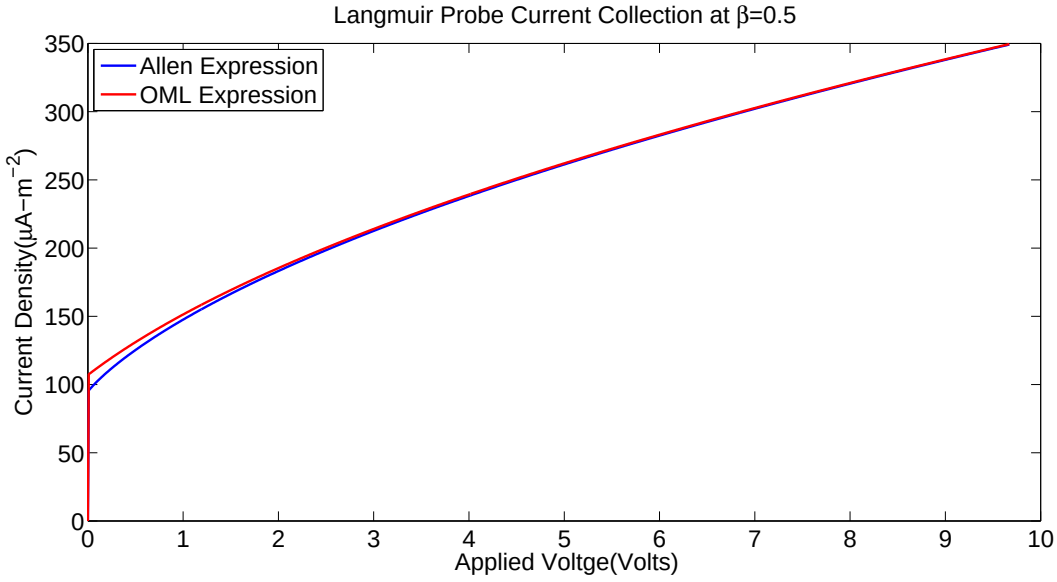

Fig. C.1: OML vs. unsimplified expression of cylindrical current collector in electron saturation region.

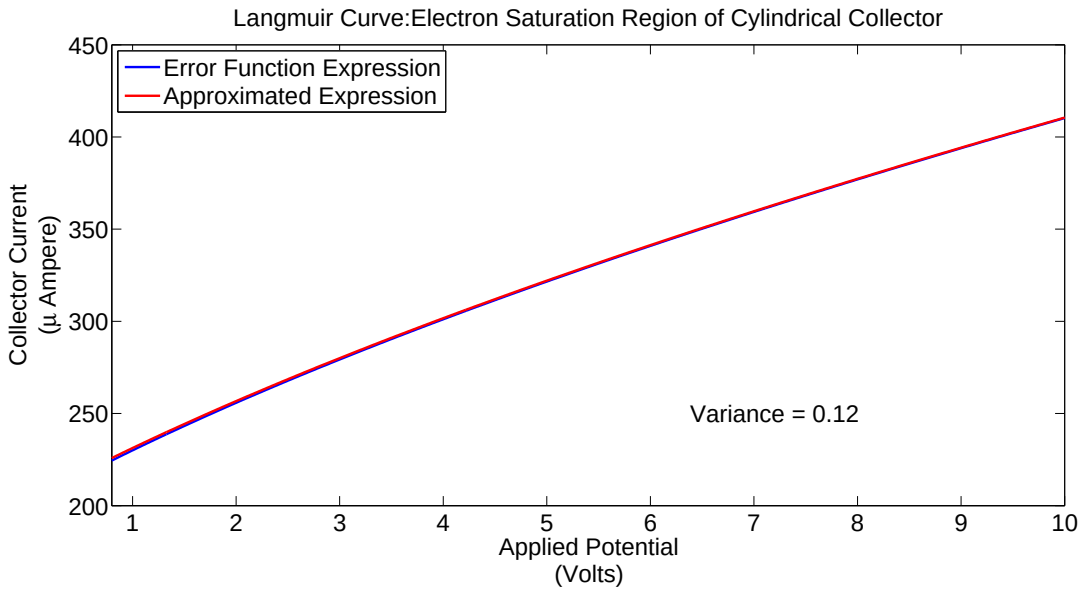

Fig. C.2: Work function variation theory: OML vs. unsimplified expression of cylindrical current collector in electron saturation region.